Site amplification, polarity and topographic effects in the Port Hills during the Canterbury earthquake sequence

A. E. Kaiser
C. Holden
C. I. Massey

GNS Science Consultancy Report 2014/121
June 2014

BIBLIOGRAPHIC REFERENCE

Kaiser, A. E.; Holden, C.; Massey, C. I. 2014. Site amplification, polarity and topographic effects in the Port Hills during the Canterbury earthquake sequence, *GNS Science Consultancy Report* 2014/121. 33 p.

CONTENTS

FIGURES

TABLES

EXECUTIVE SUMMARY

Significant permanent ground displacement and severe building damage occurred in the southern Port Hills suburbs of Christchurch during the Canterbury earthquake sequence, most notably during the Mw 6.2 February and Mw 6.0 June 2011 earthquakes. High levels of building damage and/or slope cracking occurred on hill tops in the epicentral region, indicating that local amplification of ground motions likely contributed to the most severe effects. The Canterbury earthquake sequence provides an internationally significant case study to understand the influence of topography and local stratigraphy on ground-motion amplification in hillside areas.

We present site-response analyses based on data from four small-scale temporary seismic arrays installed in the Port Hills following the 2011 February Christchurch earthquake. These arrays span generally narrow north-south trending volcanic spurs with a variety of topographic shapes. The spurs are also overlain, in part, by thick (up to 10m) loess deposits. Site amplification and polarization is assessed using H/V and site-to-reference spectral ratio methods applied to aftershocks of the Canterbury earthquake sequence. Earthquakes included in the analysis ranged in magnitude from M1.5–M5.2, hence results are based on weak-motion records

Our analyses of weak-motion scenarios, show that amplification peaks at 1–3 Hz appear to be related to slope shape. In particular, the estimated wavelength associated with this amplification is comparable to the ridge width at a given location. The strongest amplification at these frequencies generally occurs on top of narrow, steep-sided ridges (e.g., Redcliffs). We speculate that such effects may have been important during the larger events of the Canterbury sequence, during which recorded near-field ground motions were particularly rich in these frequencies.

Amplification and polarization at frequencies > 3 Hz show significant complexity over small distances (tens to hundreds of metres). In this frequency range, amplification is inferred to arise from local material impedance contrasts, and/or slope morphology, e.g., sharp convex breaks in slope.

At hillside locations, mean PGA ratios between individual array stations and a chosen reference station ranged up to a factor of 2.5 times and 3 times for horizontal and vertical motions respectively. However large inter-event variation was generally observed. Our results indicate that significant variation in horizontal and vertical PGA can occur across small distances at sites classed as rock and also from event to event. It is important to note that PGA amplification ratios derived from weak motions in this study may not be valid at stronger levels of shaking.

Our results show that both local topography and material contrasts strongly influence ground motion in the Port Hills. These observations have implications for slope stability studies and engineering design in hillside areas, given that significant amplification can occur over a broad frequency range at sites generally classed as rock according to the New Zealand design standards (NZS1170). Furthermore, much population and infrastructure in New Zealand is sited on hillside locations in areas with high seismic hazard (e.g., Wellington city).

1.0 INTRODUCTION

Current New Zealand building codes broadly classify ground-shaking hazard based on foundation soil or rock conditions (NZS1170; Standards New Zealand 2004). In general, sites on rock are expected to produce lower amplitude acceleration than soil sites, with exceptions at high frequencies (Standards New Zealand 2004). However, hillside areas generally uniformly classed as rock can also show significant amplification over a broad frequency range as well as strong local variations in high-frequency ground acceleration that are not accounted for in New Zealand design codes. Firstly, amplified ground motions can result from near-surface impedance contrasts associated with i) local surficial deposits (colluvium, alluvium etc.) or ii) highly fractured material overlying more intact materials that are typically associated with landslide-prone slopes. Secondly, focusing of seismic waves by surface morphology may result in topographic amplification near the ridge crest. A combination of both of these phenomena led to greater building damage on a prominent ridge top than at nearby soft soil sites in the 2010 Haiti earthquake (Hough et al., 2010; Assimaki & Jeong, 2013). Furthermore, the shape, and orientation of geological structures can lead to polarization effects, where ground motion is preferentially amplified in a given direction (e.g., Bonamassa & Vidale, 1991; Del Gaudio & Wasowski, 2010).

Previous seismological studies have inferred that localised amplification effects in hillside areas can have substantial control on the patterns and concentration of building and ground damage, including landslides (e.g., Harp & Jibson, 2002; Sepúlveda et al., 2005; Meunier et al., 2008; Buech et al., 2010; Hough et al., 2010). Given that such amplification effects are not taken into account in current earthquake design practice in New Zealand, more research is needed to understand their importance, in order to guide future seismic hazard mitigation efforts.

1.1 OBSERVATIONS FROM THE CANTERBURY EARTHQUAKE SEQUENCE

The Canterbury Earthquake Sequence, beginning with the Darfield Earthquake in 2010, produced the strongest ground shaking recorded in New Zealand to date (Gledhill et al., 2011; Kaiser et al., 2012). Particularly severe ground failure and building damage occurred in the southern Port Hills suburbs of Christchurch during the Mw 6.2, 22 February and Mw 6.0, 13 June 2011 earthquakes. Figure 1 shows the location of the main coseismic landslides triggered by the Canterbury earthquake sequence (modified from Massey et al., 2014a and Heron et al., 2014). Figure 2 shows the extent of building damage based on initial assessments following the February 2011 earthquake. Higher levels of building damage were generally observed in hillside areas compared to neighbouring locations on the flat-lying valley floor (distinguished by the dashed black line in Figure 2).

In general, ground-motion amplification in the Port Hills is thought to have contributed to both 1) local permanent displacement of the ground, and 2) areas of severe building damage not associated with permanent ground displacement.

1.2 SCOPE OF THIS RESEARCH

We collected new seismic data using small-scale temporary arrays at four locations in the Port Hills of Christchurch: 1) Kinsey Terrace, 2) Mount Pleasant, 3) Redcliffs, and 4) Vernon Terrace (Figure 1). This data was analysed to characterise the seismic site response and assess the extent to which amplification influenced ground motions. The majority of these sites would be uniformly classified as rock (Site class B) under NZS1170.

Here, we first assess PGA amplification factors between array stations. Secondly, we analyse amplification in terms of frequency-dependent spectral ratios. We also investigate the polarization of ground motion at each site through consideration of the variation in spectral ratios with recording axis orientation. The dependence of amplification on source direction (back-azimuth) is also briefly explored. Finally, we interpret the results in terms of topographic and stratigraphic influences on ground motion.

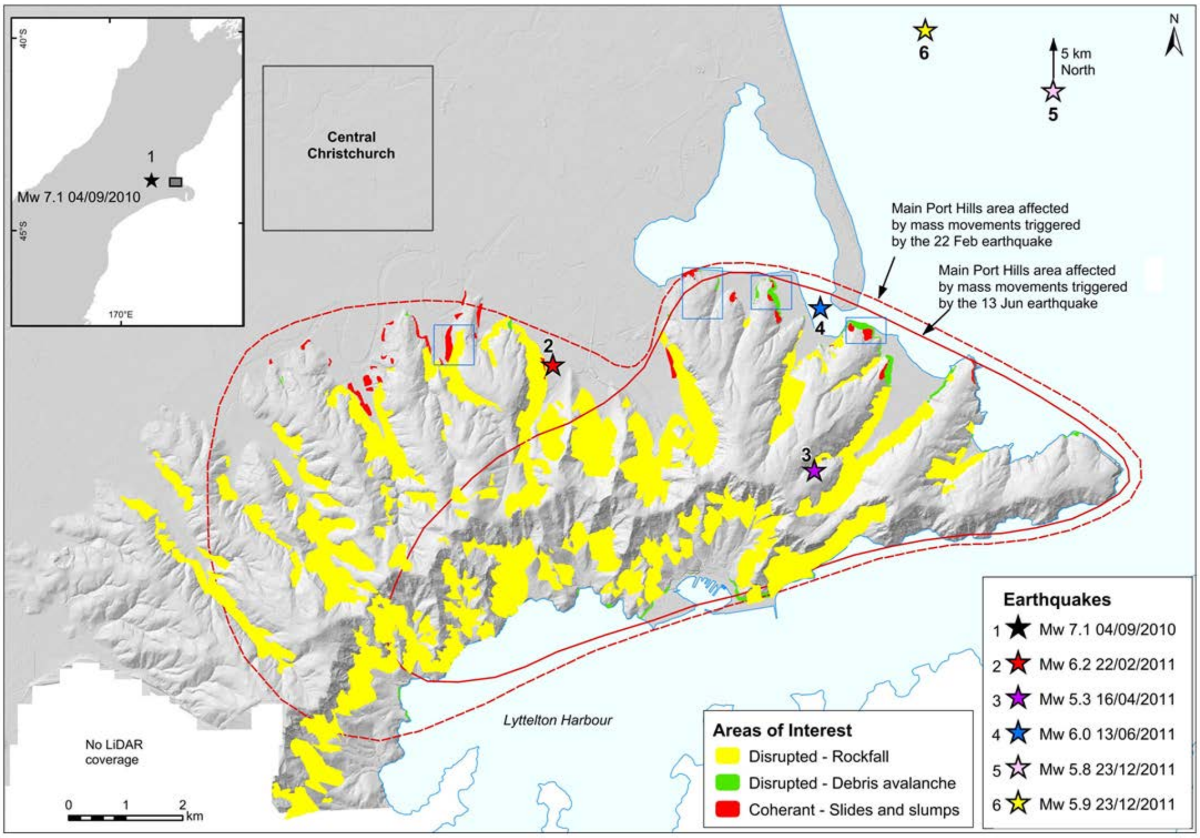

Figure 1 Map showing the location of four temporary seismometer arrays (green rectangles) and distribution of mass movements following the 22 February and 13 June 2011 Christchurch earthquakes. Data were collated from information collected by the Engineering Geology response team at GNS Science, the Port Hills Geotechnical Group and Zealand Aerial Mapping. The epicentres of the six most significant earthquakes to impact the Port Hills are shown as stars. Figure modified from Massey et al. (2014a) and Heron et al. (2014).

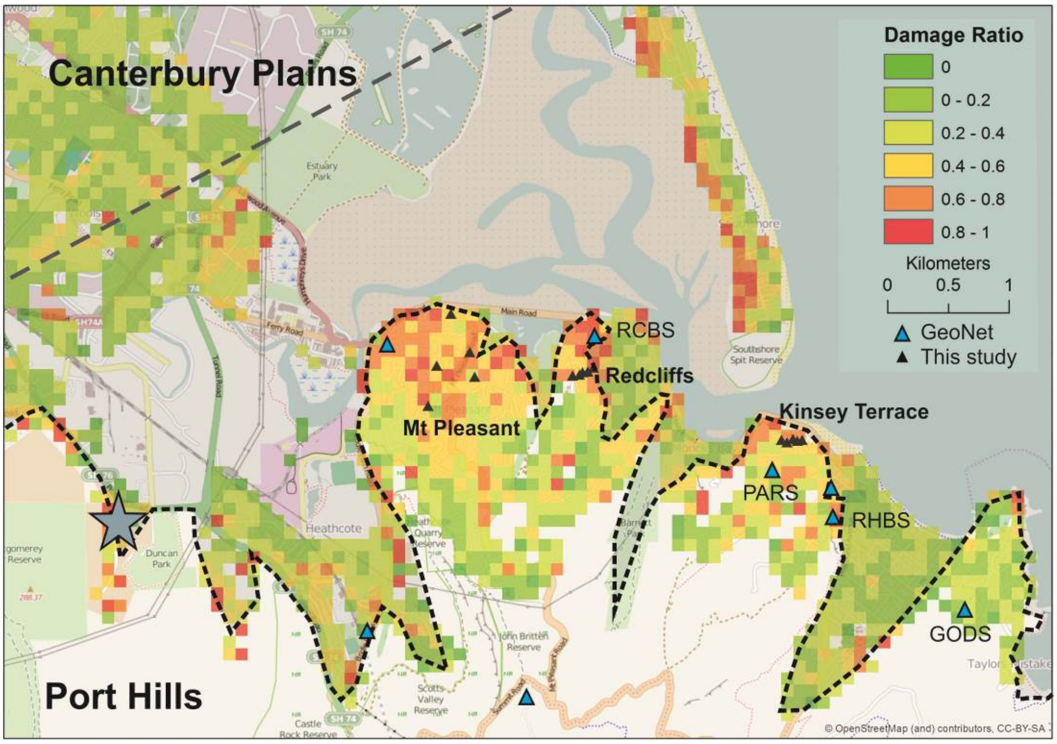

Figure 2 Spatial variability of building damage following the Mw 6.2 February 2011 earthquake (Damage map provided by Nick Horspool, GNS Science). Damage ratios are based on EQC data derived from visual street surveys conducted following the quake. Dashed black line indicates the edge of the Port Hills to the south and the Canterbury Plains to the north as defined by the surface topography. Location of array seismometers analysed in this study and GeoNet strong motion stations are shown as triangles. The epicentre and projection of the upper edge of the fault plane (Beavan et al., 2011) are indicated by the grey star and dashed line respectively.

2.0 PORT HILLS ARRAYS

2.1 GEOLOGY AND GEOMORPHOLOGY

The Port Hills form the northern flank of the extinct volcano of Banks Peninsula (up to 500m above sea level). The basaltic rocks of the Port Hills belong to the Lyttelton Volcanic Group of Miocene age (10–12 Myrs old; Forsyth et al., 2008) and are mantled by much younger deposits derived from wind-blown sand and silt (loess) and colluvial deposits of mixed local rock debris and re-worked loess (Bell & Trangmar, 1987). These deposits are usually at least 1 m thick and locally more than 10 m thick (Bell & Trangmar, 1987; Massey et al., 2013; 2014a). Major land damage in the Port Hills from the February and June 2011 earthquakes (classified according to Hungr et al., 2014) included: rockfalls; loess slides, falls and flows; loess-and-rock slides, falls and flows (e.g., Kinsey Terrace); rock slides, topples, falls and debris avalanches (e.g., Redcliffs) as well as soil “toe” slumps (e.g., Vernon Terrace).

Following the Mw 6.2 February 2011 earthquake, 1-Hz short-period Lennartz sensors were deployed by GNS Science in small-scale temporary aftershock arrays at four hillside sites (locations Figure 1; detail Table 1). Each array consisted of five instruments spanning a range of topographic and/or stratigraphic features. The geology of the sites is summarised in Table 1 and Massey et al. (2013) and described in the following sections. Topographic profiles at each site are shown in Figure 3.

Table 1 Summary of the four small-scale seismometer arrays.

Array	Local Geology/Topography	Date In	Date out	Earthquakes analysed
Kinsey Terrace	A north-south trending ridgeline terminating in a steep (>60°) abandoned coastal cliff (since c. 1840). Formed in mixed volcanic rocks overlain by thick deposits (4–14 m in parts) of loess. Permanent ground movement (loess/rock slide) is towards the east and extends from below the ridge crest to the cliff edge. Many houses damaged due to permanent ground deformation.	09.06.2011	19.01.2012	443 M 1.9–4.7
Redcliffs	A north-south trending ridgeline terminating in a steep (>60°) abandoned (c. 3500 yr) coastal cliff. Formed in mixed volcanic rocks. Cliff edge on the eastern side corresponds to a sharp break in slope. Significant shaking damage to houses near cliff edge. Significant rock falls, slides, topples and debris avalanches have occurred from the steep rock slope.	31.03.2011	27.04.2011	207 M 1.9–4.3
Mt Pleasant	A north-south trending ridgeline formed in mixed volcanic rocks, thinly mantled with loess, fill and colluvium (< 1 m thick). High shaking damage to residential houses – no significant permanent ground deformation.	10.03.2011	31.03.2011	216 M 1.5–4.2
Vernon Terrace	Low angle slopes (~25°) near the valley bottom formed in mixed colluvium, loess and alluvium. Some shaking damage to houses but many damaged by permanent ground deformation associated with a soil “toe” slump.	27.04.2011	09.06.2011	132 M 1.8–5.2

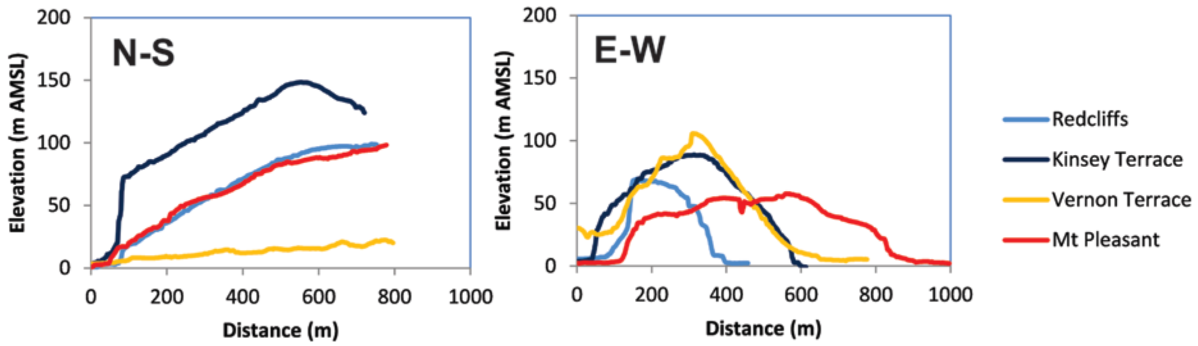

Figure 3 Topographic cross sections north-south and east-west through the array sites.

2.1.1 Kinsey Terrace

The Kinsey Terrace array (Figure 4), spans an area of complex deformation relating to a coherent (after Keefer, 1984) soil/rock slide in both loess and rock. Here, coseismic permanent displacements recorded by continuous GPS and cadastral surveys (total horizontal displacement of ~1 m) appear to be primarily sub-parallel and down dip of the volcanic sequences (towards bearing 070°–080°), suggesting a low-angle translational failure mechanism within the soil and rock. Many of the residential properties on the displaced area were significantly damaged. The array stations K1–K3 are within the landslide and above approximately 4–10 m of loess. Array stations K4 and K5 are off the landslide, and are on weathered rock with a thin (less than 1 m) loess cover.

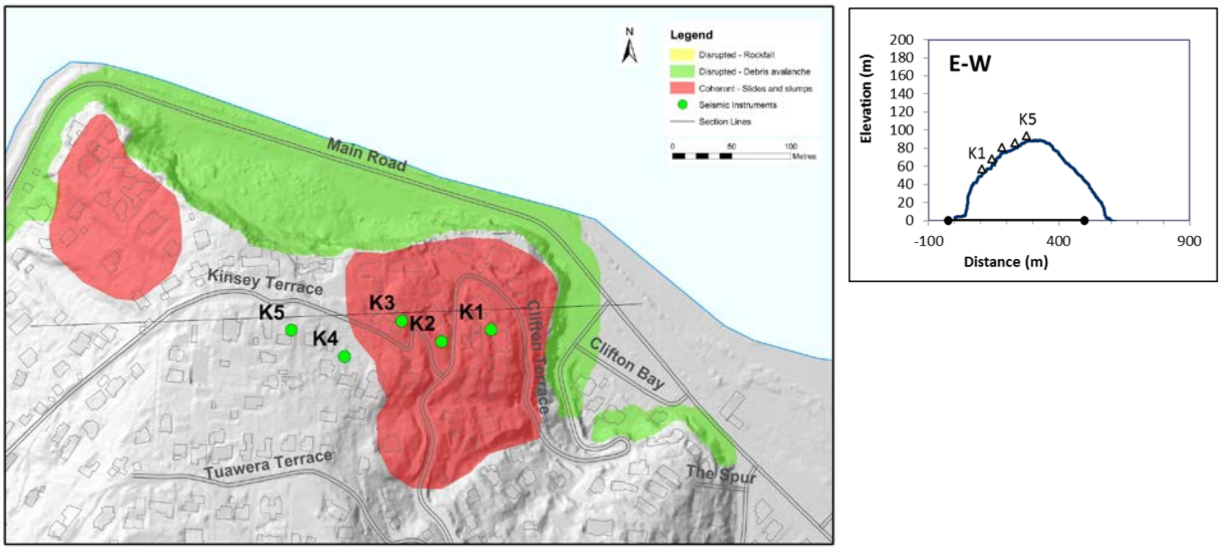

Figure 4 Kinsey Terrace array map (left) and sketch of elevation profile (right). The portion of the E-W elevation profile marked by the black line segment corresponds to the black line cross-section in map view. Approximate station locations (triangles) are shown projected onto elevation profile.

2.1.2 Redcliffs

During the 22 February 2011 earthquake, two people were killed by falling rock at Redcliffs; one person was in a dwelling and another was in their garden, both at the bottom of the slope in the debris runout zone.

The Redcliffs array (Figure 5), transects an asymmetric north-trending spur with a very steep eastern flank (cliff face) and a gentler sloping western flank. The width and height of the spur are about 300 m and 80 m respectively. The cliff on the eastern side is about 70 m high, 500 m long with a slope angle ranging from 60° to overhanging in places. The cliff has three main sections based on slope aspect: 1) a southern, northeast-facing cliff; 2) a central, southeast-facing cliff; and 3) a northern north east-facing cliff. The southern and central parts of the cliff are the steepest and the array was installed perpendicular to the cliff crest in the steepest part of the cliff.

Array stations R2–R5 are predominantly sited on weathered rock (with a thin < 1 m cover of loess). Station R1 is on weathered rock with a thin (1–2 m) cover of loess, and is sited within a zone of cracking associated with the permanent coseismic deformation of the rock slope and loess at the cliff crest.

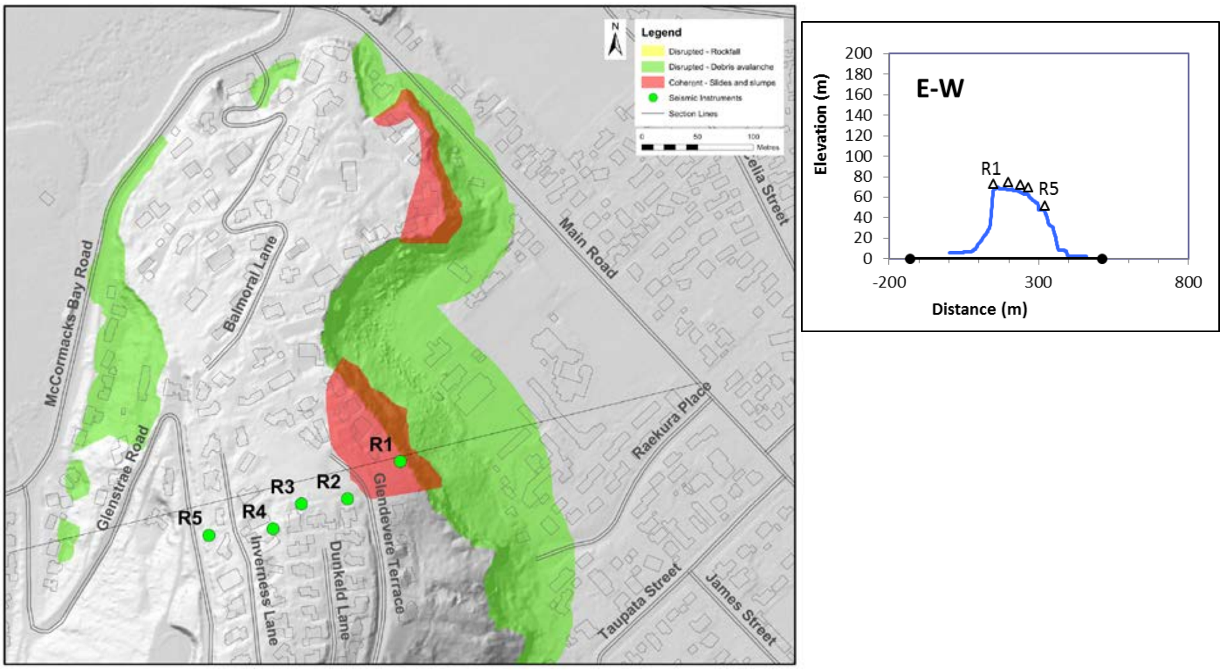

Figure 5 Redcliffs array map (left) and sketch of elevation profile (right). The portion of the E-W elevation profile marked by the black line segment corresponds to the black line cross-section in map view. Approximate station locations (triangles) are shown projected onto elevation profile.

2.1.3 Mt Pleasant

The Mount Pleasant array (Figure 6), spans a rock slope overlain by mixed loess and colluvial deposits. Here, no evidence of large permanent ground failure was observed, even though residential properties and retaining walls were significantly damaged by ground shaking. Array stations M1–M3 and M5 are all sited on weathered rock, while M4 is sited on >5 m of soil, assumed to be remobilised loess and alluvium.

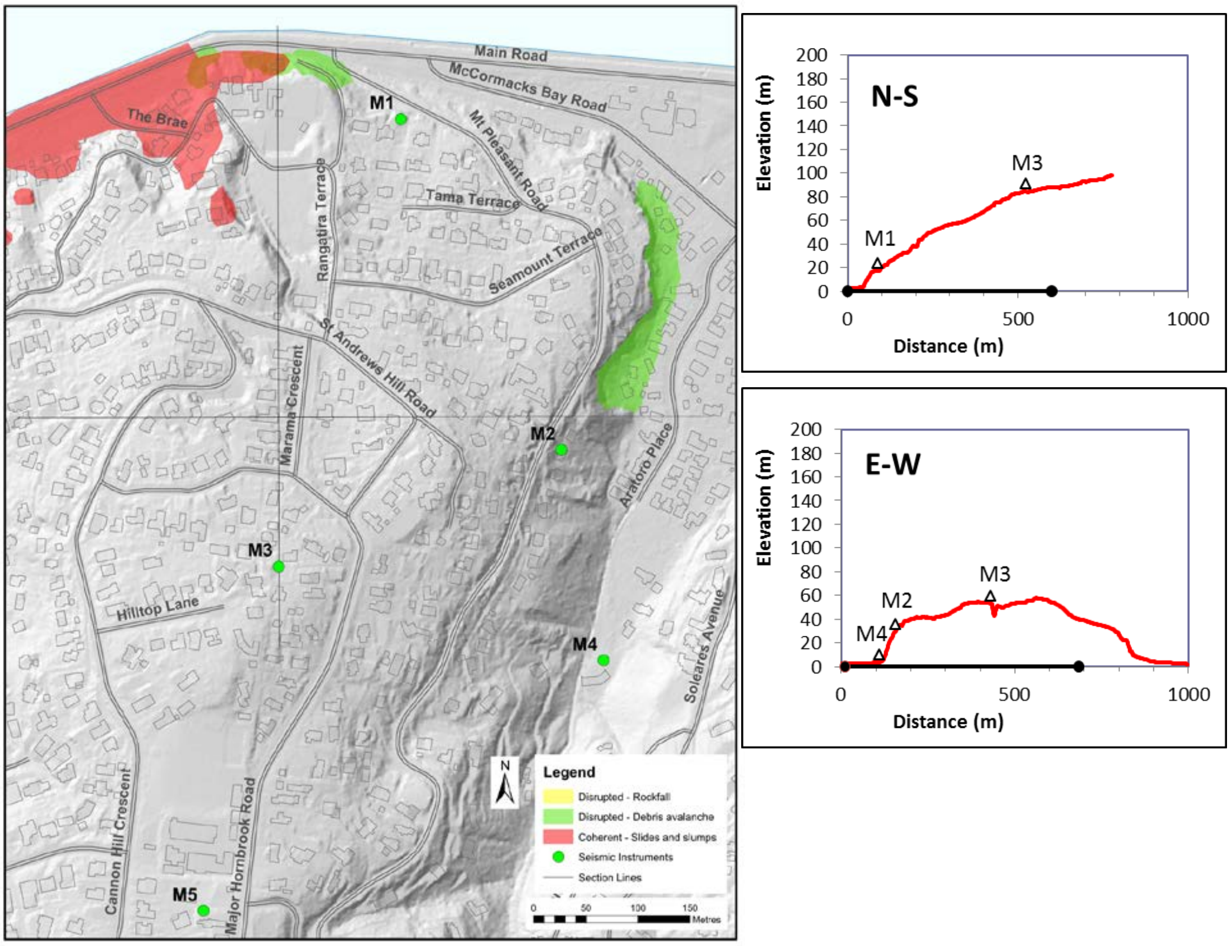

Figure 6 Mt Pleasant array map (left) and sketch of elevation profiles (right). The portion of the E-W and N-S elevation profiles marked by the black line segments, correspond to the black line cross-sections in map view. Approximate station locations (triangles) are shown projected onto elevation profile.

2.1.4 Vernon Terrace

The array at Vernon Terrace (Figure 7), is perpendicular to a low-angle slope, spanning a coherent soil “toe” slump. Stations V2–V5 are located on loess and loess colluvium, which increases in thickness from V2 (about 5–10 m thick) to V5 (>15 m of mixed loess, colluvium and alluvium) at the valley bottom. Array station V1 is on rock, with a thin (< 1 m) cover of loess.

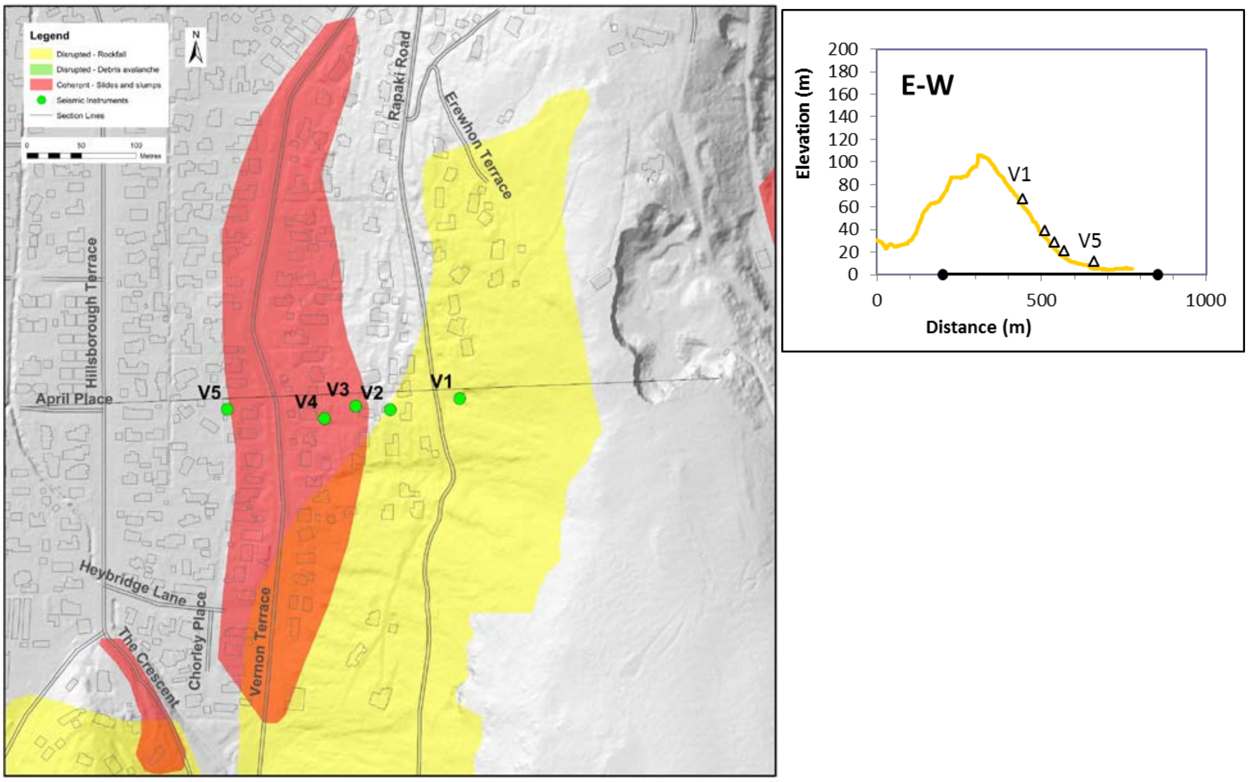

Figure 7 Vernon Tce array map (left) and sketch of elevation profiles (right). The portion of the E-W elevation profile marked by the black line segment corresponds to the black line cross-section in map view. Approximate station locations (triangles) are shown projected onto elevation profile.

2.2 SEISMIC DATA

The arrays combined recorded more than 1000 small to moderate-sized earthquakes (M1.5–M5.3) for use in this study. Details of the recording period at each array are given in Table 1.

For each array, data were extracted for all earthquakes located by the GeoNet network within the Christchurch region, as well as earthquakes greater than magnitude 4.5 in the wider Canterbury area. Only earthquakes recorded satisfactorily at all stations of the array were used in the analysis and are shown in Figure 8. Note, that although the June Mw 6.0 earthquake occurred during the Kinsey deployment, records from this earthquake and other nearby large aftershocks could not be used because of amplitude clipping associated with the recording instruments. Each array recorded over one hundred earthquakes fitting the criteria above over a range of source back-azimuths (see Figure 8).

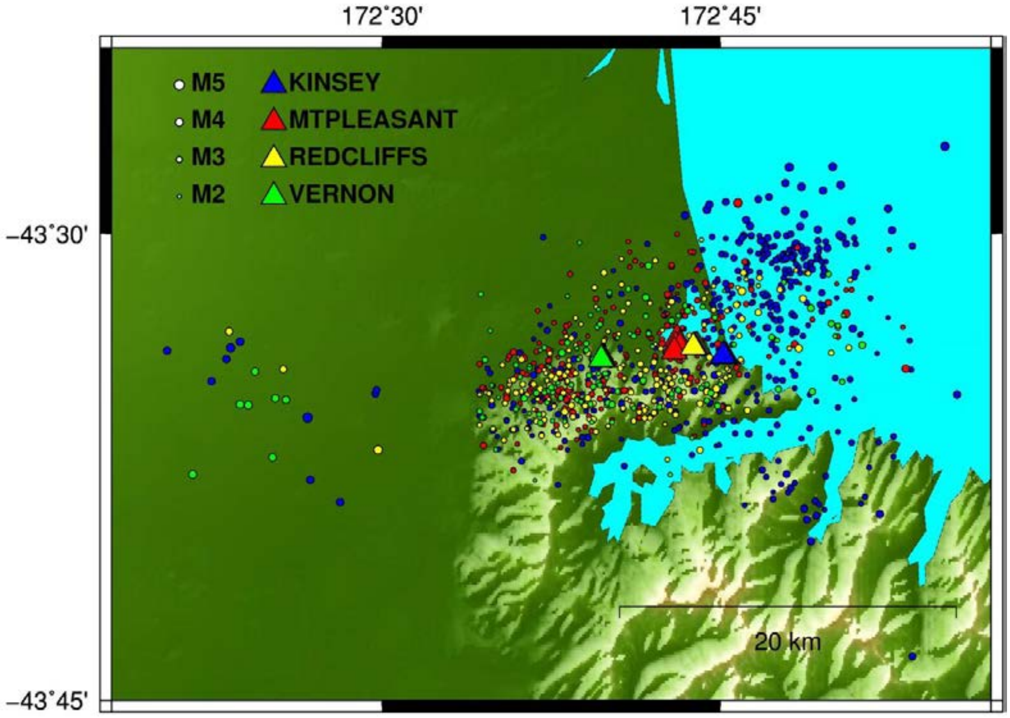

Figure 8 Earthquakes used in the spectral analysis color-coded according to the recording array.

2.3 PRELIMINARY ARIAS INTENSITY ANALYSIS PRIOR TO THIS REPORT

Previously, preliminary analysis of the array data from Kinsey Terrace and Mt Pleasant was carried out by analysing azimuthally-varying Arias intensity during a selection of events ranging from M2.3–M4.3 (Kaiser et al., 2013a). Arias intensity is easily calculated from the time series by taking the time-integral of the acceleration squared over the duration of the record. It provides an energy-based measure of intensity that takes into account motions over the full duration of the seismic record and has been used for correlation with slope failure.

Results from the Port Hills arrays presented in Kaiser et al. (2013a) showed significant variability in Arias intensity across small inter-station distances (tens to hundreds of metres). Variability was observed in terms of both amplification and polarization of the maximum Arias intensity. At Kinsey Terrace differences in Arias intensity of factors of 3 to 5 times were found at sites located within the landslide damage zone compared to stations on stable rock. Furthermore Arias intensities showed a dominant polarization direction specific to each site that was independent of source back-azimuth (Kaiser et al., 2013a; Holden et al., 2014). This suggests that the dominant polarization is controlled by site conditions rather than source effects.

The preliminary results presented in Kaiser et al. (2013a) provided some useful insights into the role and variability of site effects at our array locations. However, this work is limited by the fact that Arias intensity also depends strongly on the particular earthquake source used in the analysis. During large damaging earthquakes, a much broader range of frequencies will be excited than during the earthquakes used in this study, hence site effects at lower frequencies will become much more important. To better assess site amplification and polarization across the broad frequency band (0.5–20 Hz) likely to contribute to damage in hillside suburbs, more applicable spectral ratios methods and results have been used in this report.

3.0 METHODS

Peak ground acceleration (PGA) is the ground-motion parameter directly related to coseismic landslide initiation (Wartman et al., 2013). We first compared relative PGA at all stations within a single array as an initial assessment of ground-motion amplification. PGA amplification factors were calculated relative to a reference station. The reference station was chosen by considering both the array station exhibiting the lowest average PGA over the events studied as well as giving preference for stations located in areas likely to be less influenced by amplification, i.e., on stable rock away from the ridge crest or any significant breaks in slope. While, the reference station was thus chosen to be as free of amplification effects as possible, in some cases no ideal reference station was available, as discussed in the following section.

Second, both single-station horizontal-to-vertical (H/V) ratios and site-to-reference (S/R) spectral ratios were calculated to evaluate frequency-dependent amplification.

Shear-wave spectra used to calculate the spectral ratios were calculated based on a five second window beginning 0.5 s before the S-wave arrival and smoothed using a Konno & Ohmachi (1998) windowing function for the frequency range 0.5–20 Hz. H/V and S/R spectral ratios were then calculated for each individual earthquake and the geometric mean of the ratios is presented in this report (e.g., Figure 9).

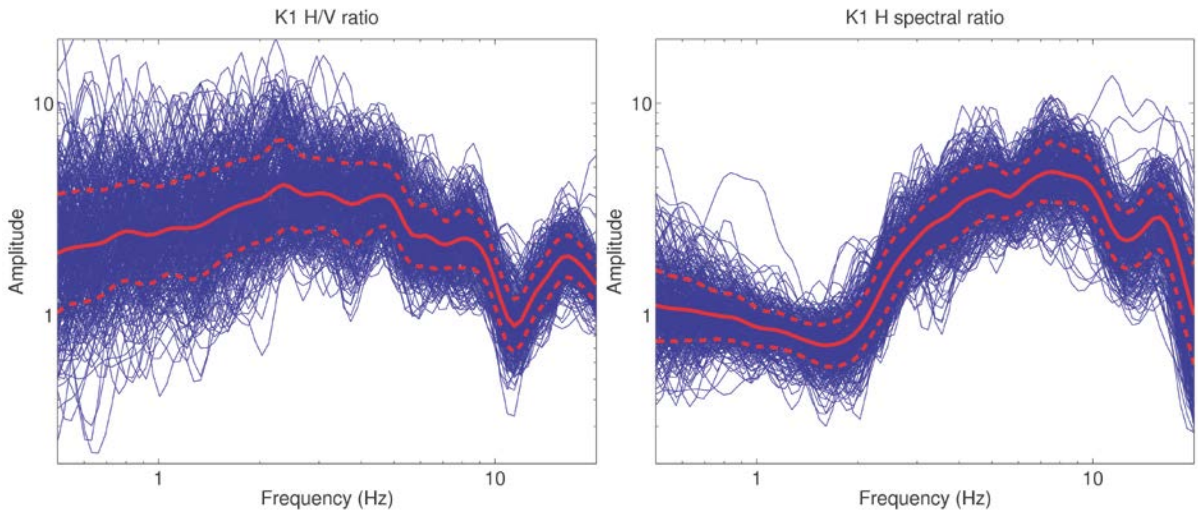

Figure 9 Example H/V (left) and site-to-reference (right) spectral ratios plotted for individual earthquakes (blue lines). Geometric mean (red solid line) and standard deviations (red dashed lines) represent the ratio distribution. K1 spectral ratio is with respect to reference station K5.

H/V methods are useful for determining the resonance frequency of large-scale features at lower frequencies and tend to be common across all stations of the small-scale array. However, H/V methods may be biased by amplification of the vertical component, especially at higher frequencies (e.g., Parolai et al., 2004).

In contrast, site-to-reference spectral ratios provide a clear indication of high-frequency effects that differ between stations. Although they may be biased by amplification effects at the reference station, they provide a much more robust analysis of local-scale effects originating from small-scale features at each station. For this method, the reference station was chosen to be the station exhibiting the smallest PGA and the flattest H/V ratio over the frequency range up to 10 Hz.

Preferential polarization of ground motion was assessed by considering both H/V and site-to-reference ratios for azimuths of the recording axes oriented every 10°.

The influence of source back-azimuth on ground-motion amplification was investigated by considering how the maximum H/V amplification in the critical 1–5 Hz frequency range varied with source back azimuth for the recorded events.

4.0 RESULTS

4.1 PGA AMPLIFICATION

Peak ground acceleration (PGA) was compared between individual stations and a chosen reference station at each site in Figure 10. Results show significant differences in mean PGA amplification between stations up to 2.7 times horizontal and 3.7 times vertical (observed at shallow soil sites at Vernon Terrace). Considering rock sites only, the mean PGA amplification factors ranged up to 2.5 for horizontal motions (at Redcliffs station R2), and up to 3 for vertical motions (at Mt Pleasant station M3). However, there was significant variation in these values across individual events, as seen from the range of values within one standard deviation of the mean shown in Figure 10. Furthermore, these values are derived from small to moderate sized earthquakes dominated by high-frequency ground motions and therefore they cannot be considered appropriate for larger magnitude shaking without further study. The applicability of these factors to large damaging events is uncertain, due to the broader frequency range of ground motion excited during larger magnitude earthquakes and possible nonlinear site effects. Nevertheless, PGA amplification factors observed here illustrate the significant variation in ground acceleration in both horizontal and vertical directions across small distances at sites considered as rock according to the NZS1170 standard.

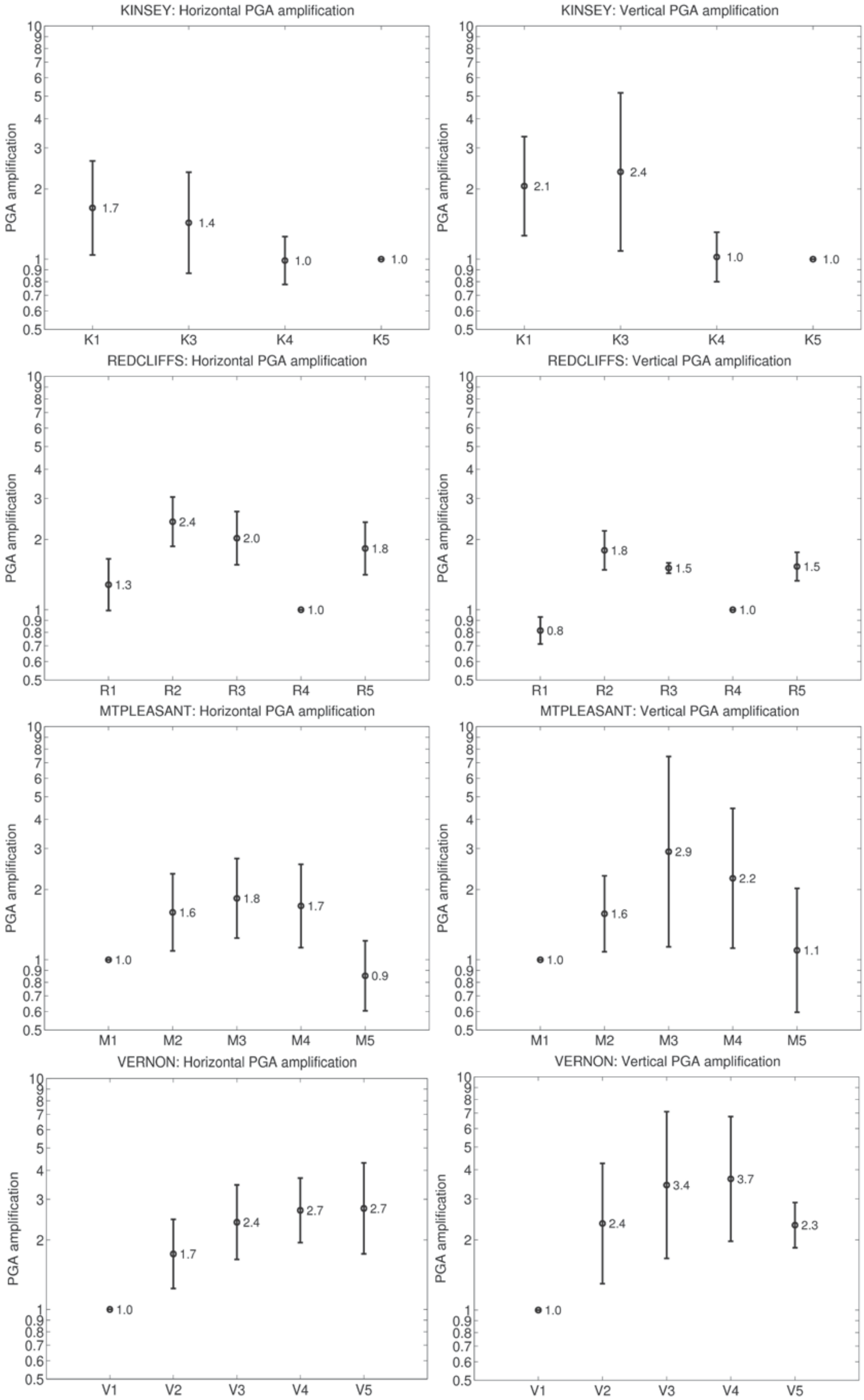

Figure 10 PGA amplification with respect to the reference station in the horizontal (left) and vertical (right) directions. The horizontal PGA is taken to be the larger of the two horizontal components. Geometric mean and standard deviations of the amplification factors across individual events are shown as error bars.

4.2 KINSEY TERRACE

The Kinsey array stations (labelled K1 to K5) are distributed on an E-W transect across the area of significant landslide movement (Figure 4). K2 did not return robust data for use in this study due to issues in the recording stage. K5 located on stable rock close to the ridge crest exhibited the lowest amplitude across the frequency range of interest and was chosen as the reference station for the site-to-reference spectral ratios.

Figure 11 and Figure 12 summarize the H/V spectral ratios calculated for different orientation axes. Clear amplification at 1–2.2 Hz is evident at all stations with a consistent peak at 1.6 Hz. Amplification factors are approximately 3.5. This is similar in character to the observed amplification at GeoNet station PARS on the crest of the same ridge ~300 m further to the south, although the amplification at PARS is somewhat lower in frequency (0.7–1.5 Hz; Kaiser et al., 2013b). Figure 11 and Figure 12 show amplification extends up to higher frequencies at station K1 and K3.

Site-to-reference spectral ratios shown in Figure 13 illustrate strong amplification up to 7 times at stations within (K1, K3) compared to outside (K4, K5) the landslide deformation area. This amplification occurs at frequencies greater than 2 Hz for horizontal motions. Notably, vertical motions are also amplified up to 4 times at frequencies greater than 3 Hz. The significant vertical amplification at stations K1 and K3 (Figure 13) suggests that horizontal amplification at these frequencies is underestimated in the H/V ratio at this station. The strong amplification at K1 and K3 is inferred to arise from an increased shallow velocity contrast where weaker material within the deformation zone overlies more intact (stronger) rock.

The H/V azimuthal variations (Figure 11) show amplification is associated with weak polarization in the NNW-SSE direction at all stations. This polarization is slightly stronger at stations on the landslide (K1 and K3). The polarization direction is perpendicular to the steepest slope direction, the main bearing of landslide displacement, and observed surface cracking (Figure 4). This is consistent with the observations of Moore et al. (2011) who found polarization perpendicular to displacement of an unstable rock mass in Switzerland was caused by preferentially oriented tensional fractures associated with the slope instability. At Kinsey, polarization is observed at K4 and to a lesser extent K5, suggesting that tensional fracturing of underlying rock may extend outside the main area of landslide displacement. Furthermore, topographic amplification leads to preferential polarization of ground motion in the ridge-perpendicular direction (e.g., Hartzell et al., 2014). At Kinsey, the larger ridgeline is oriented N-S before turning NE-SW further to the south. The array also spans a smaller NE-SW oriented spur with a significant cliff to the north. The shape of the local topography is also likely to give rise to preferential polarization in the NW-SE or E-W directions, although the complexity of the topography makes this difficult to fully evaluate.

The polarization results presented here are improved from preliminary results presented in Kaiser et al. (2013a). Results may differ due to the fact the previous Arias intensity analysis tended to reveal high-frequency polarization only, due to dominant frequencies associated with the small earthquakes used in the analysis.

The relationship between amplification and source back-azimuth is illustrated in Figure 14. Hartzell et al. (2014) found amplification is greater when the source is aligned with the major axis of the ridge, particularly for frequencies above the fundamental resonance mode of the ridge (for Kinsey Tce, this is assumed to correspond to the peak at 1.6 Hz; see discussion section). Our study suggests that maximum amplification in the 1–5 Hz frequency range (up to a factor of 8) occurs at station K1 for sources to the northeast. This direction is approximately perpendicular to the preferred polarization direction. However, the same effect is not seen for sources located to the southwest. Other stations show no significant dependence on source back-azimuth and overall the influence of source back-azimuth is significantly less than that of local site conditions.

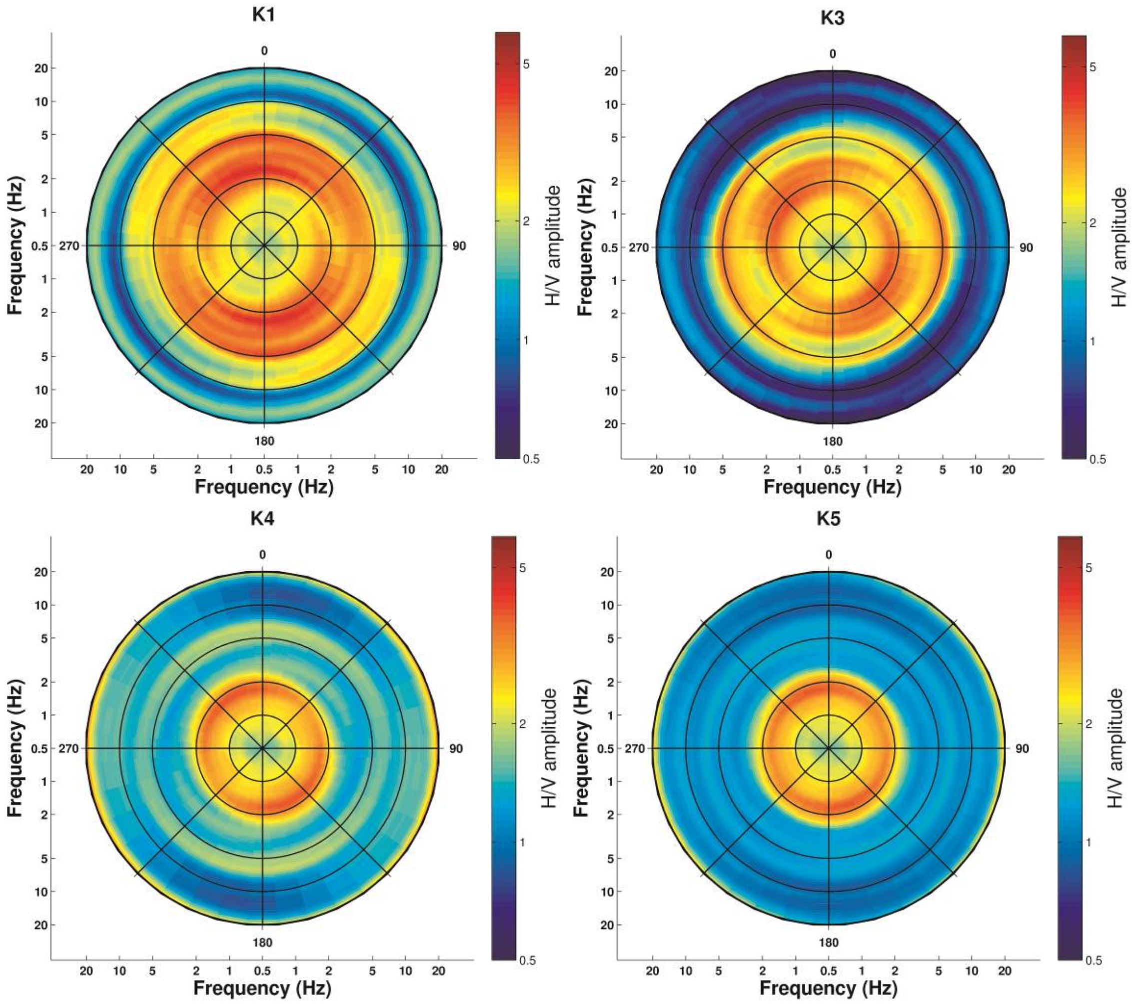

Figure 11 H/V analysis at Kinsey Terrace. Polar plots illustrate azimuthal variations in amplification depending on recording axis. Strong amplification is observed at 1–2 Hz at stations K4 and K5 and in a wider frequency band (up to 6 Hz) at stations K1 and K3 within the deformation area.

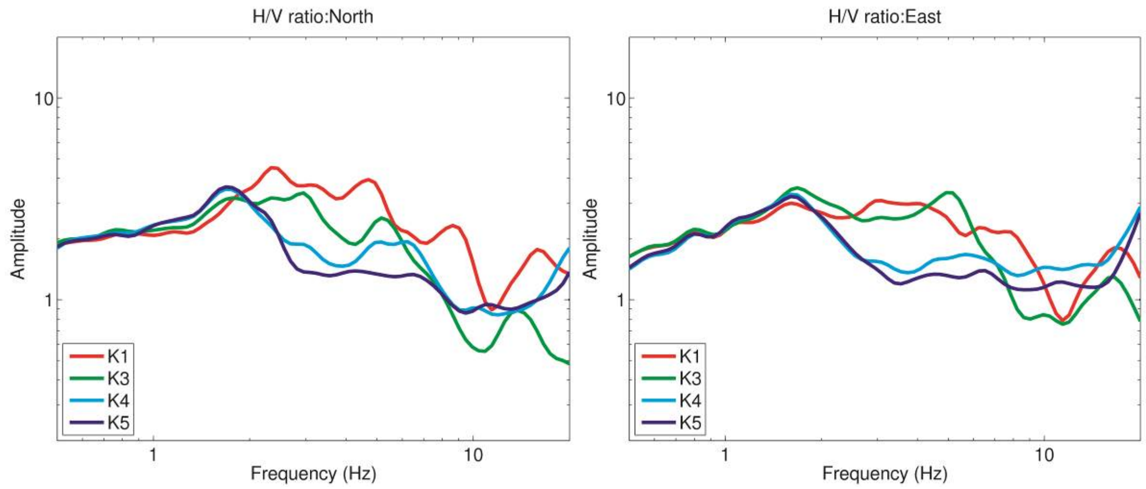

Figure 12 Kinsey Terrace H/V ratios compared at each station in the north and east directions.

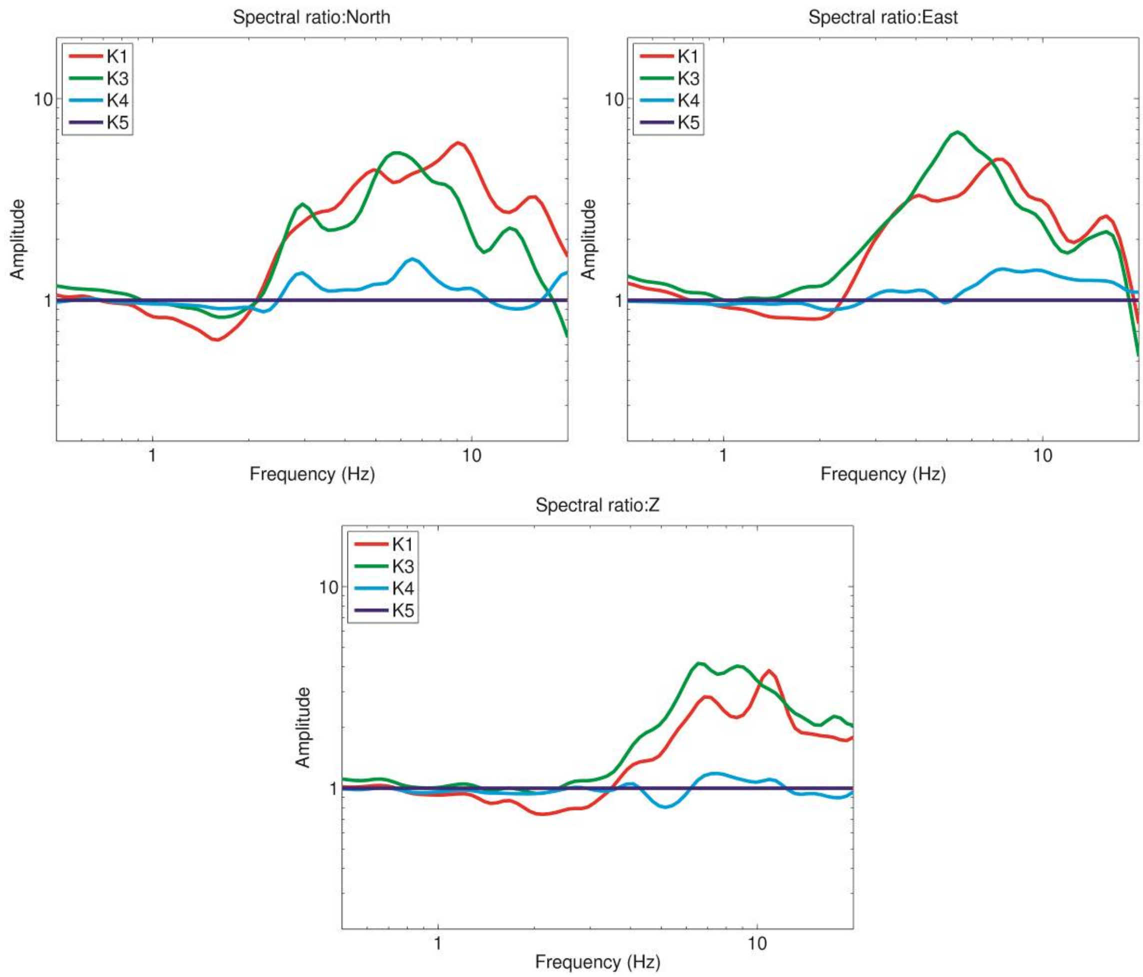

Figure 13 Kinsey Terrace spectral ratios with respect to reference station K5 for three orthogonal components.

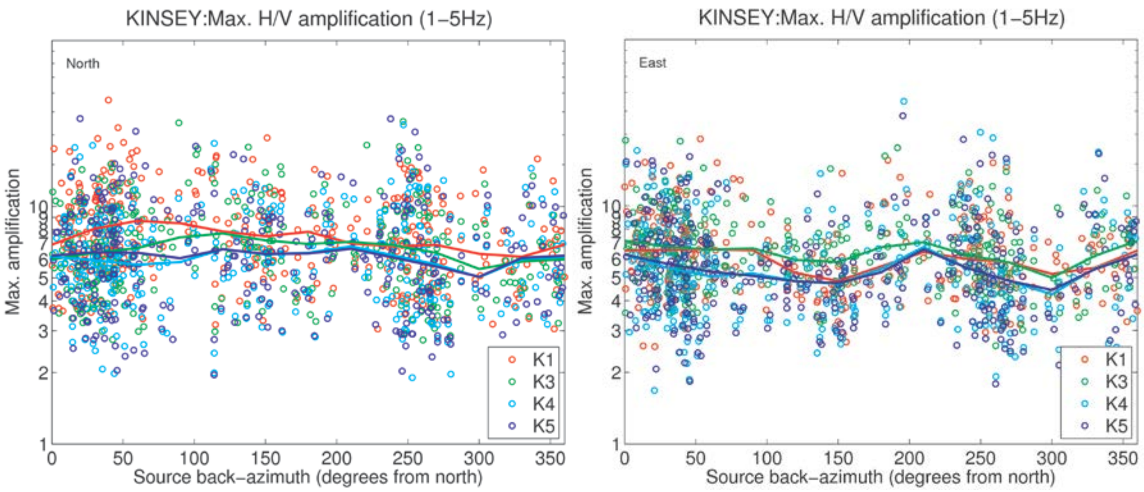

Figure 14 Amplification vs. source backazimuth. Amplification is the maximum given by individual H/V ratios in the 1–5 Hz frequency range. Plots are shown for amplification in the north (ridge parallel, slope perpendicular) and east (ridge perpendicular, slope parallel) directions. Solid lines show the geometric mean within overlapping windows spaced every 30 degrees. At Kinsey Terrace, no significant variations in maximum amplification are seen with source back-azimuth.

4.3 REDCLIFFS

The Redcliffs array transects a narrow flat-topped approximately N-S trending ridge bounded to the east by a sharp NW-SE striking cliff edge (Figure 5). Given all stations lie close to the ridge top, there is no ideal reference station for the Redcliffs array. Station R4 was chosen as the reference for spectral ratio calculation because it generally had the lowest amplitude recordings and was located on flatter ground at the top of the ridge away from sharp breaks in slope.

H/V ratios from Redcliffs (Figure 15 and Figure 16) show strong and consistent amplification at 1–2 Hz at all sites. Peak amplification occurs at 1.5–1.6 Hz and is significantly more pronounced in the local ridge/cliff perpendicular direction (approx. 40°). Amplification factors are up to 7 times in the cliff-perpendicular direction compared to up to 3.5 times in the approximately ridge-parallel direction.

Spectral ratios with respect to R4 (Figure 17) show greater amplification up to 6 times at the cliff-edge station R1 at frequencies between 1.5–5 Hz, centred at 3 Hz. This amplification, while particularly pronounced in the ridge-perpendicular direction, is also evident on the ridge-parallel and vertical components. Amplification of vertical motions at R1 indicates true amplification factors are likely to be higher at these frequencies than is suggested by the H/V ratio. At station R5 at the western change in slope, amplification in the horizontal directions is similar in character to that at R1 but has significantly lower amplitude.

Analysis of source back-azimuth (Figure 18) suggests that earthquakes in line with the ridge to the south and to the NW tend to produce higher maximum amplification (up to 9–12 times) at all stations in the ridge perpendicular direction. By contrast maximum amplification in the ridge-parallel direction does not appear to be strongly influenced by source back-azimuth, with the possible exception that earthquakes to the north tend to excite lower amplification, although this is poorly constrained by the available data.

Topography clearly controls the main amplification features at this site. Higher frequency amplification at station R1 and to some extent R5 is inferred to be associated with the strong breaks in slope at these stations. Station R1 is also located within the zone of cracking associated with deformation of the weathered rock slope and overlying loess (1–2 m at the station) at the cliff edge during the major earthquakes (Figure 5). At Redcliffs, severe damage to houses at the cliff crest during the February 2011 earthquake (Figure 2) is consistent with the strong amplification observed at this site.

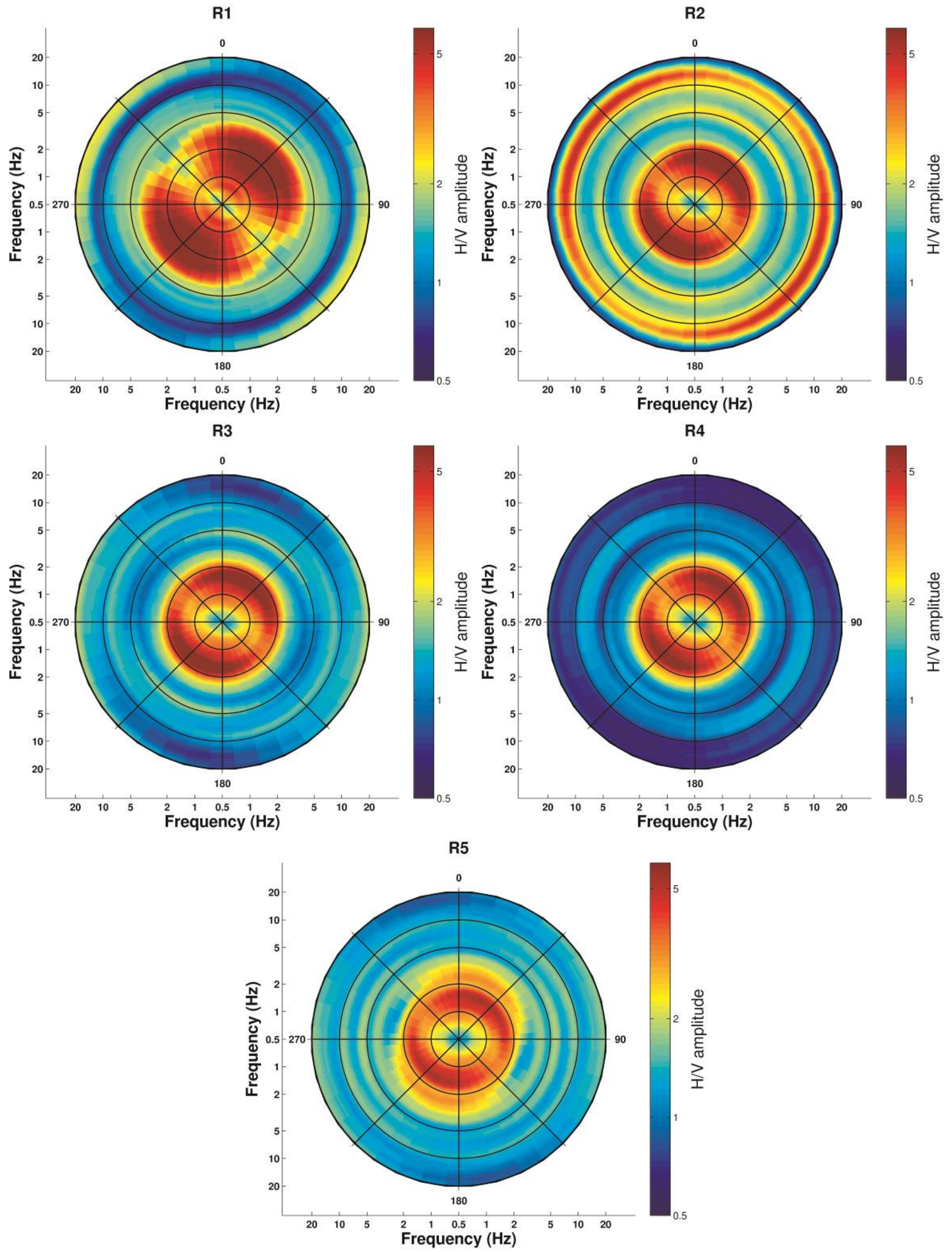

Figure 15 H/V analysis at Redcliffs. Polar plots illustrate azimuthal variations in amplification depending on recording axis. Strong amplification is observed at 1–2 Hz at all stations and is associated with preferential polarization of ground motion in the NE-SW direction (ridge-perpendicular) direction.

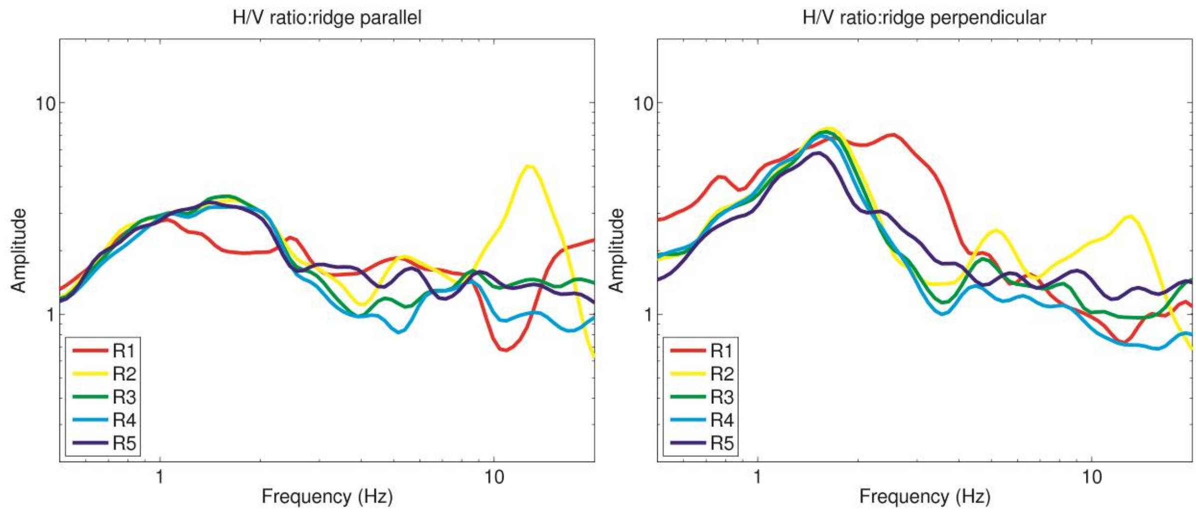

Figure 16 Redcliffs H/V ratios compared at each station in the ridge-parallel (130°) and ridge-perpendicular (040°) directions.

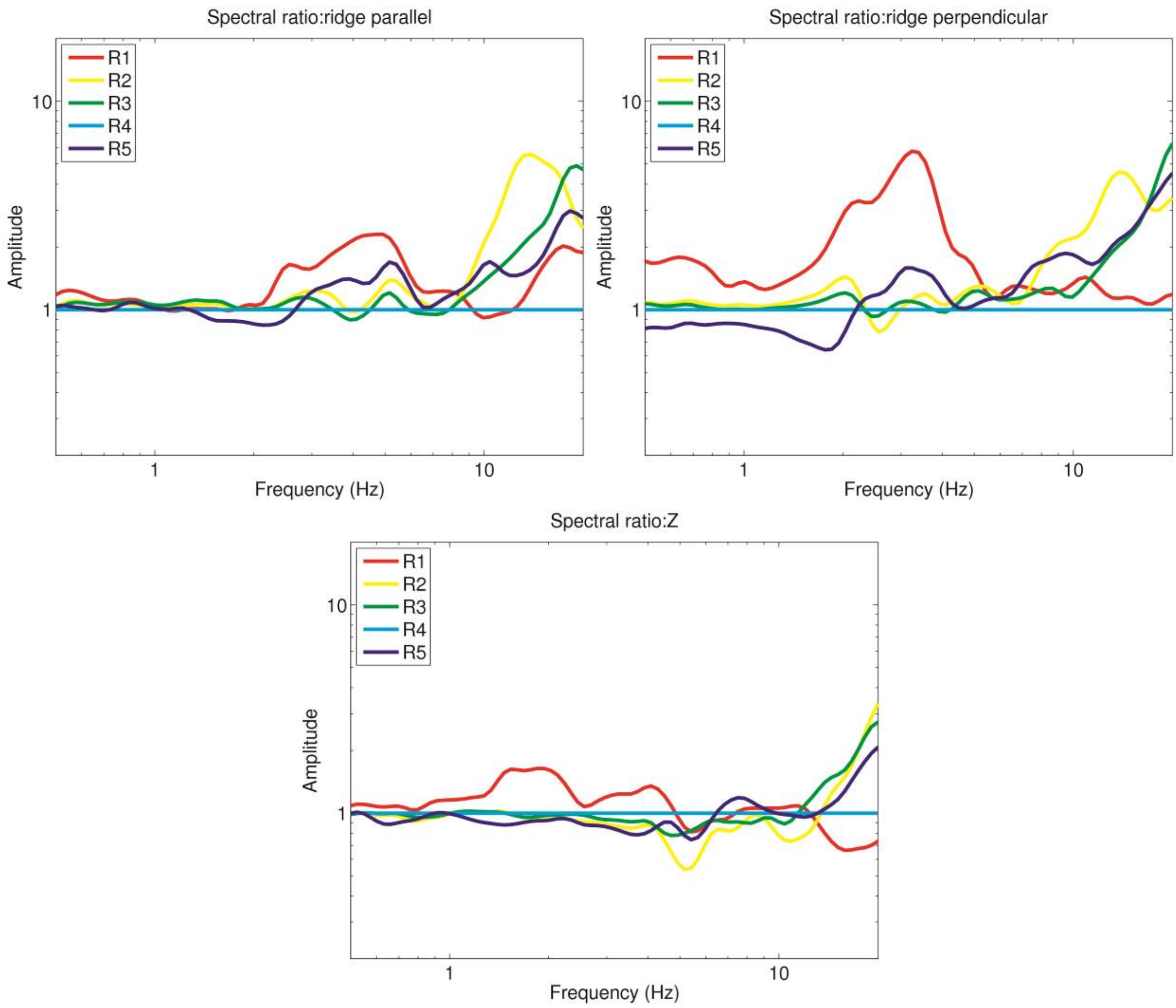

Figure 17 Redcliffs spectral ratios with respect to reference station R4 for three orthogonal components.

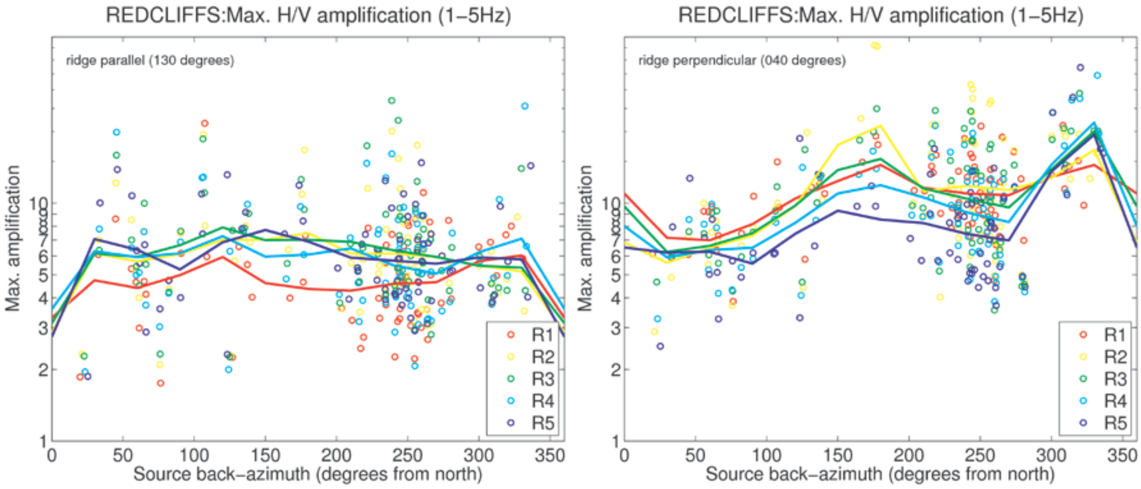

Figure 18 Amplification vs. source back-azimuth. Amplification is the maximum given by individual H/V ratios in the 1–5 Hz frequency range. Plots are shown for amplification in the ridge-parallel (130°) and ridge-perpendicular (040°) directions. Solid lines show the geometric mean within overlapping windows spaced every 30 degrees. Strongest ridge-perpendicular amplification occurs with source back-azimuths of ~180° and ~320°).

4.4 MT PLEASANT

The Mount Pleasant stations (M1–M5) are distributed along the top and side of a broad north-south striking ridge, that slopes gently downwards towards the north (Figure 6). In general, the station spacing (> 200 m) at this array is greater than at the other Port Hills arrays and the site conditions are more variable. Station M1 was chosen as the reference station because it exhibited generally low amplitude records and was situated close to the base of the slope.

H/V ratios (Figure 19 and Figure 20) and spectral ratios (Figure 21) show variable amplification across all stations, particularly at high frequencies. H/V amplification factors for frequencies below 3 Hz are lower than the previous sites, ranging between 2–3 times and tend to be weakly polarized in the N-S direction at stations along the main axis of the ridge (M1, M3 and M5). Analysis of source back-azimuth (Figure 22) suggests the N-S amplification may be stronger across the array during earthquakes to the south, but results are not statistically significant and reasons for this apparent variation are unclear. Earthquakes to the north tended to be generally associated with amplification and polarization in the E-W direction, particularly at the northernmost station M1. This observation is consistent with previous studies of topographic amplification. Spectral ratios (Figure 21) show amplification at frequencies below 3 Hz is somewhat less at station M4 in the local stream gully than at stations along the major axis of the ridge, although the amplification peak is still apparent in the H/V ratio.

Both spectral ratios and H/V ratios illustrate strong high-frequency local amplification effects at stations M4 (~7 Hz), M3 (~10 Hz) and M2 (~14 Hz). Each of these stations appears to have a distinctive peak frequency not observed at other stations. These effects could be associated with higher mode topographic amplification, but are more likely to be local effects associated with the immediate subsurface conditions or sensor installation.

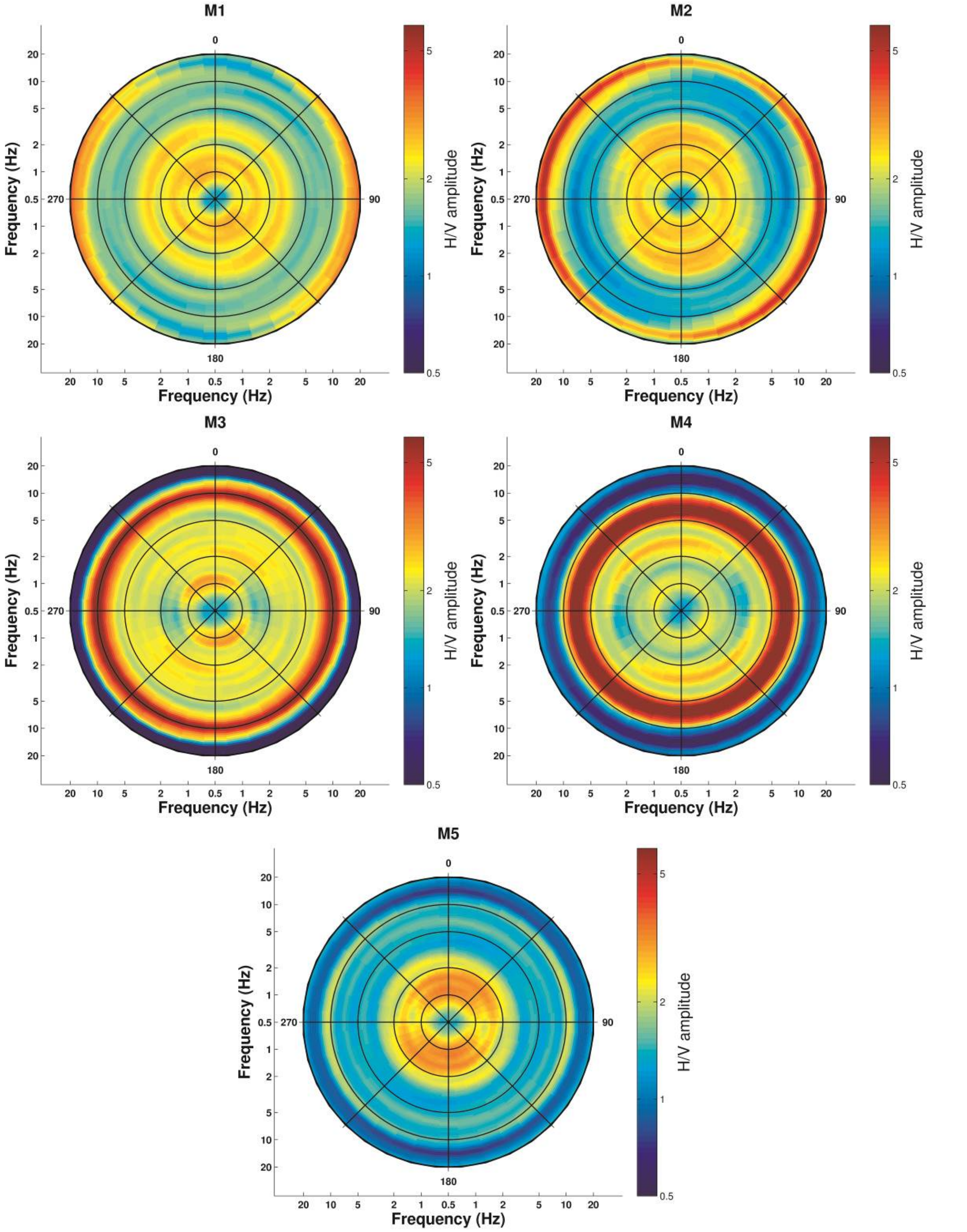

Figure 19 H/V analysis at Mt Pleasant. Polar plots illustrate azimuthal variations in amplification depending on recording axis. Strong and variable amplification is seen across the array, with preferential polarization consistently in the north-south (ridge-parallel) direction for frequencies between 1–3 Hz.

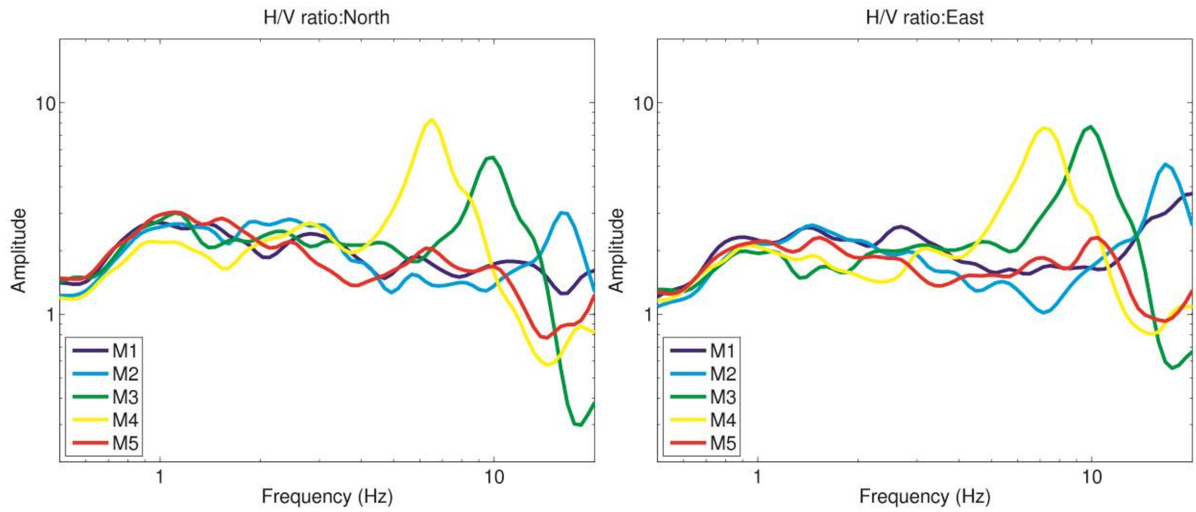

Figure 20 Mt Pleasant H/V ratios compared at each station in the north (ridge parallel) and east directions (ridge perpendicular).

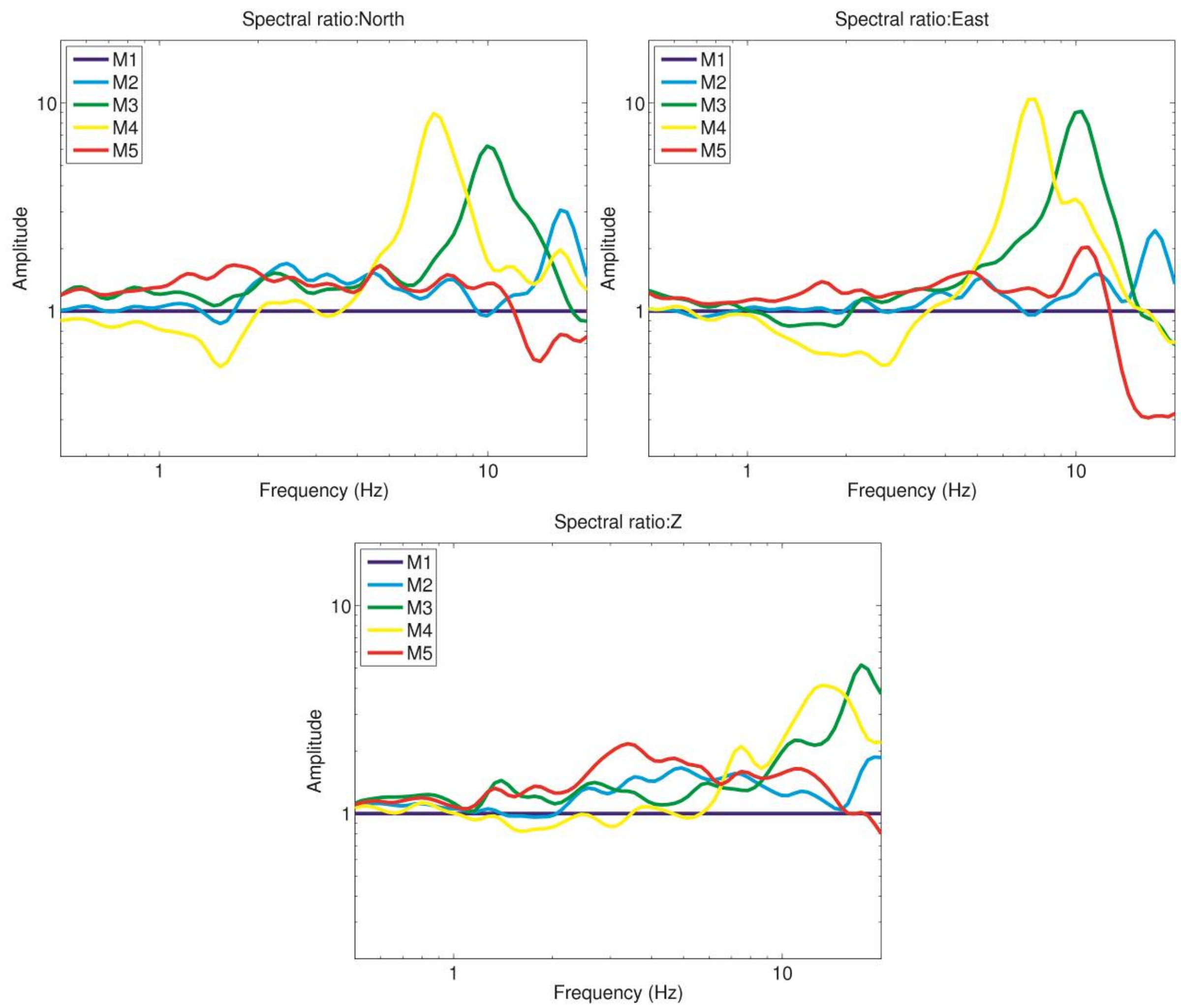

Figure 21 Mt Pleasant spectral ratios with respect to reference station M1 for three orthogonal components.

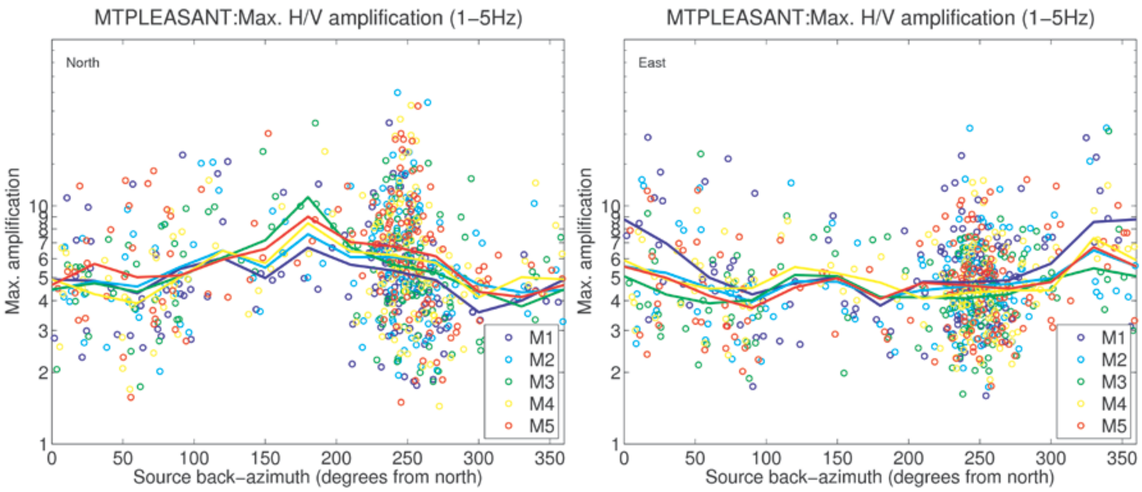

Figure 22 Amplification vs. source back-azimuth. Amplification is the maximum given by individual H/V ratios in the 1–5 Hz frequency range. Plots are shown for amplification in the north (ridge parallel) and east (ridge perpendicular) directions. Solid lines show the geometric mean within overlapping windows spaced every 30 degrees.

4.5 VERNON TERRACE

The array at Vernon Terrace spanned a coherent slump in predominantly loess at the basin-edge where the Port Hills rise above the Canterbury Plains (Figure 7). The reference station, V1, was located on weathered rock half-way up a steep N-S trending ridgeline. Stations V2–V5 were located progressively further downslope on landslide/soil deposits increasing in thickness. Station V5 was located not far above the level of the Canterbury Plains in a small incised valley.

H/V ratios (Figure 23 and Figure 24) show amplification at ~1 Hz at stations V1–V4, which is likely related to the ridge topography. Station V5 shows broader low-frequency amplification likely associated with the influence of the Canterbury basin (i.e., Kaiser et al., 2013b) and a strongly N-S polarized peak at 2 Hz that may be associated with the local valley or shallow soil structure. Complex amplification patterns that vary between sites are observed in the H/V ratio at higher frequencies and are better assessed using site-to-reference spectral ratios.

Spectral ratios (Figure 25) clearly illustrate the shift in amplification towards lower frequencies with increasing soil depth downslope (i.e., from V2 to V5). Peak amplification factors range from 6–10 times and peak frequencies with respect to station V1 range from ~7 Hz at V2 to ~4Hz at V5. This shift in frequency is particularly evident on the slope-parallel component, whereas the slope-perpendicular component shows significantly greater amplification at station V3 and significantly less at station V5. Notably, vertical amplification occurs up to 6–7 times at all stations with respect to V1.

Analysis suggests H/V amplitudes between 1–5 Hz are largely independent of source back-azimuth (Figure 26).

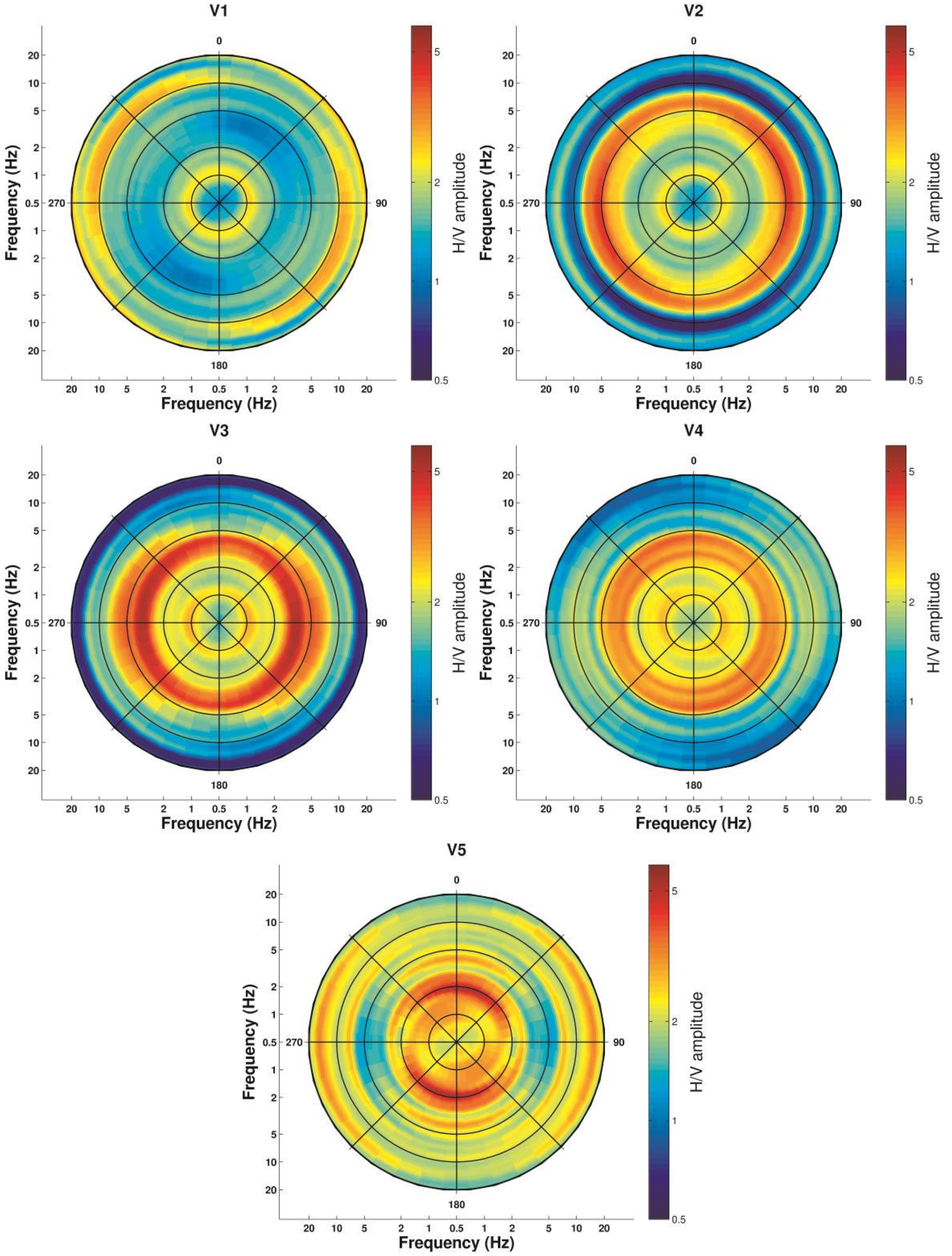

Figure 23 H/V analysis at Vernon Terrace. Polar plots illustrate azimuthal variations in amplification depending on recording axis. Strong amplification is observed at stations on the landslide with increasingly lower frequencies from the reference station (V1) down-slope to the slope toe (V5).

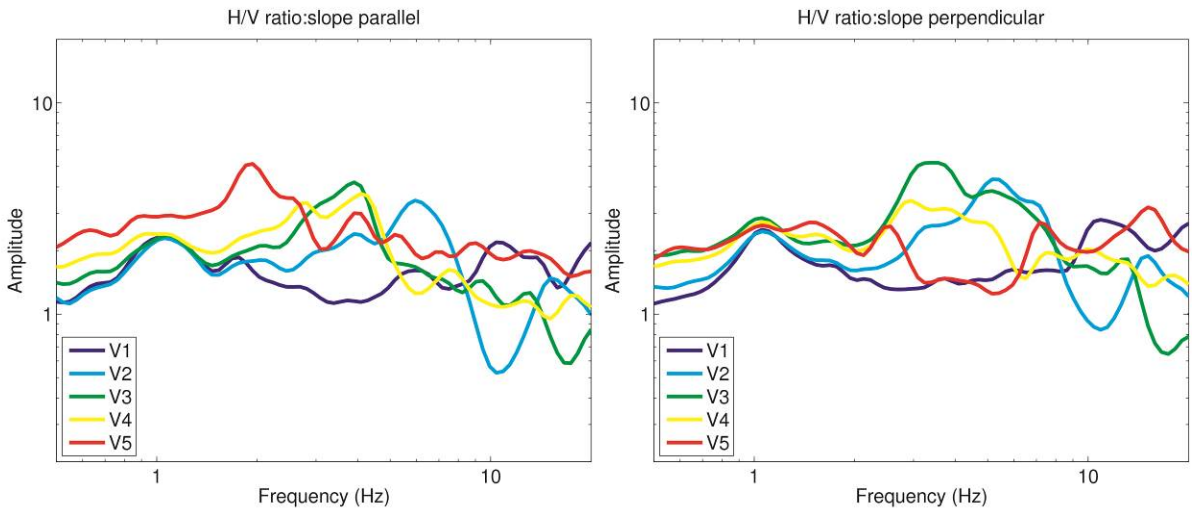

Figure 24 Vernon Terrace H/V ratios calculated in the slope-parallel (north) and slope-perpendicular (east) directions.

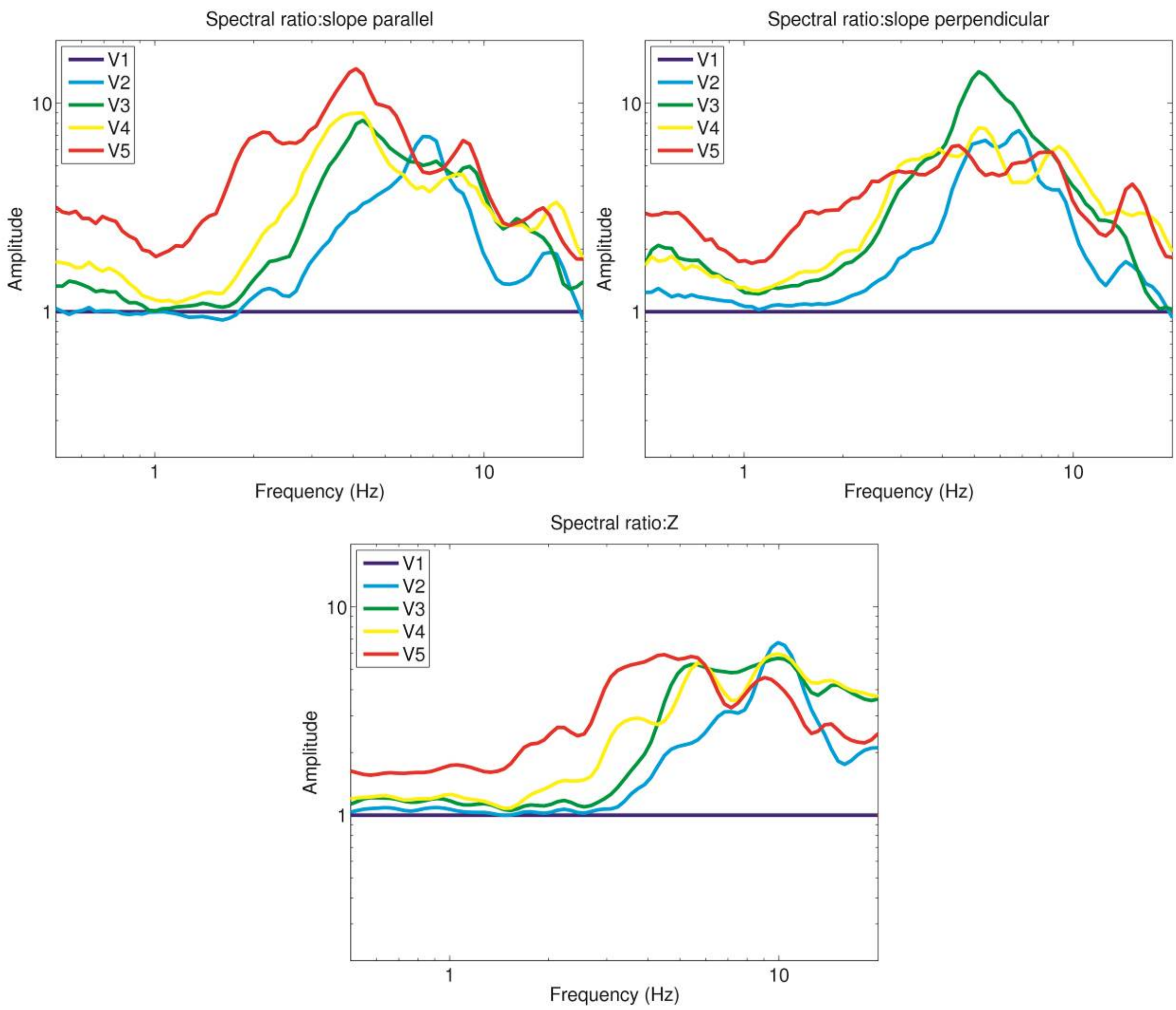

Figure 25 Vernon Terrace spectral ratios with respect to reference station V1 for three orthogonal components.

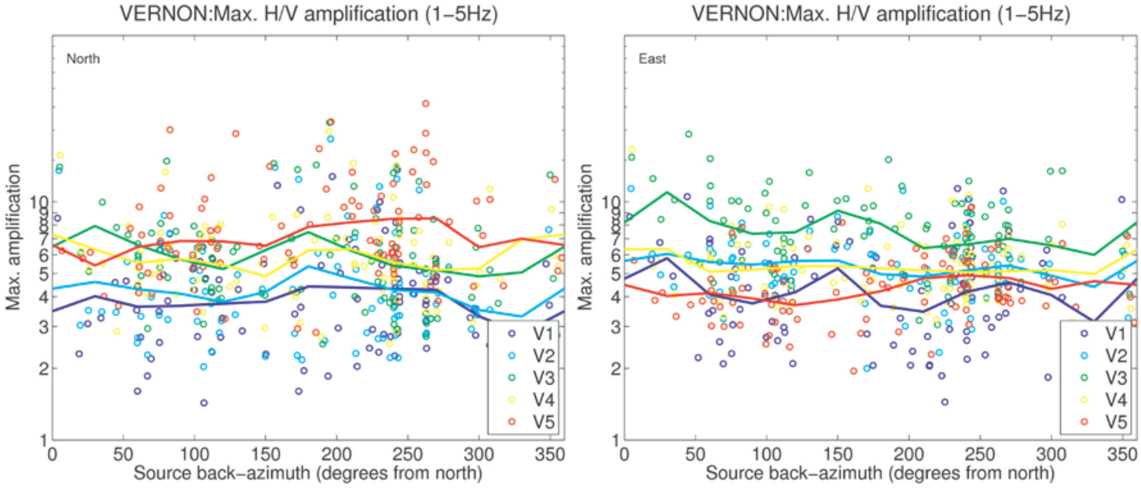

Figure 26 Amplification vs. source back-azimuth. Amplification is the maximum given by individual H/V ratios in the 1–5 Hz frequency range. Plots are shown for amplification in the north (ridge-parallel) and east (ridge-perpendicular) directions. Solid lines show the geometric mean within overlapping windows spaced every 30 degrees.

5.0 DISCUSSION

The lowest frequency amplification peak observed in H/V ratios occurred within the 1–3 Hz range at ridge-top locations at all sites. The frequency of amplification appears to be related to ridge width. The review by Geli et al. (1988) suggests that hill-crest amplification occurs for wavelengths comparable to the width of the hill. In Figure 27, we investigate this relationship for the Port Hills.

To evaluate the relationship between the lowest observed amplification peak and the ridge dimension, we take the observed frequency of amplification and assume an average shear-wave velocity of 1000 m/s for basalt lava and basalt lava breccia comprising the Port Hills (based on downhole measurements ranging from 600 m/s to > 2000 m/s detailed in Massey et al., 2014b from Richmond Hill site RHBS (location shown in Figure 2). The approximate wavelength of amplification is then calculated from these values and compared to the ridge width in Figure 27. Additional results from Kaiser et al. (2013b) for national network GeoNet stations are also included in this figure.

Figure 27 shows that the observed wavelength of the H/V amplification peaks correlates strongly with ridge width. Values are comparable, but tend to be somewhat larger than the ridge width. Our results are governed by our assumption of uniform shear-wave velocity of 1000 m/s and may also be influenced by unaccounted for vertical amplification biasing the H/V ratio. In our study, a better match between observed amplification wavelength and ridge width would require the bulk shear-wave velocity to be lower (approximately 800 m/s, which is entirely consistent with the range of down-hole shear-wave measurements for basalt lava breccia found in the Port Hills). This would suggest that relatively low-velocity rock comprises the Port Hills and is expected to enhance topographic amplification effects in this region.

The degree of amplification in the 1–3 Hz range indicated by H/V ratios (shown by colours in Figure 27) was particularly strong at sites located on steep, narrow ridgelines, e.g., Redcliffs, and GeoNet stations RHBS and GODS. This is consistent with conclusions that topography at the ridge scale plays a role in ground motion amplification.

Amplification was also found to extend to higher frequencies (> 3Hz) at local cliff edges and sharp breaks in slope (e.g., at Redcliffs). This amplification was associated with strong polarization in the ridge perpendicular direction (also perpendicular to local tensional cracking). In addition, local soil deposits or weakened rock associated with unstable slopes was also found to play a significant role in amplifying ground motion in this frequency range (e.g., Kinsey Tce, Vernon Tce, and Redcliffs).

The source back-azimuth was also a factor that likely influenced ground-motion amplification at Redcliffs, although it was less important than the site conditions. Amplification at this site tended to be greatest when sources were aligned with the major ridge axis, leading to preferential amplification in the ridge-perpendicular direction. This is consistent with expectations from previous studies. No significant dependence on source back-azimuth was found at the other sites.

The results presented in this study show amplification in the Port Hills is related to both topographic shape at the ridge scale, and the relatively low velocity material that comprises the eastern Port Hills. It is also influenced at higher frequencies by local material contrasts and sharp breaks in slope. More detailed 2D modelling is being undertaken at selected sites in the Port Hills (e.g., Massey et al., 2014b), which will enable us to better quantify the relative contribution of these factors to ground motion amplification. Importantly the largest Canterbury earthquakes were rich in energy in the 1–5 Hz range (Kaiser et al., 2012; Ristau et al., 2013) such that amplification effects in the Port Hills are likely to have had a significant influence on ground motions during these events.

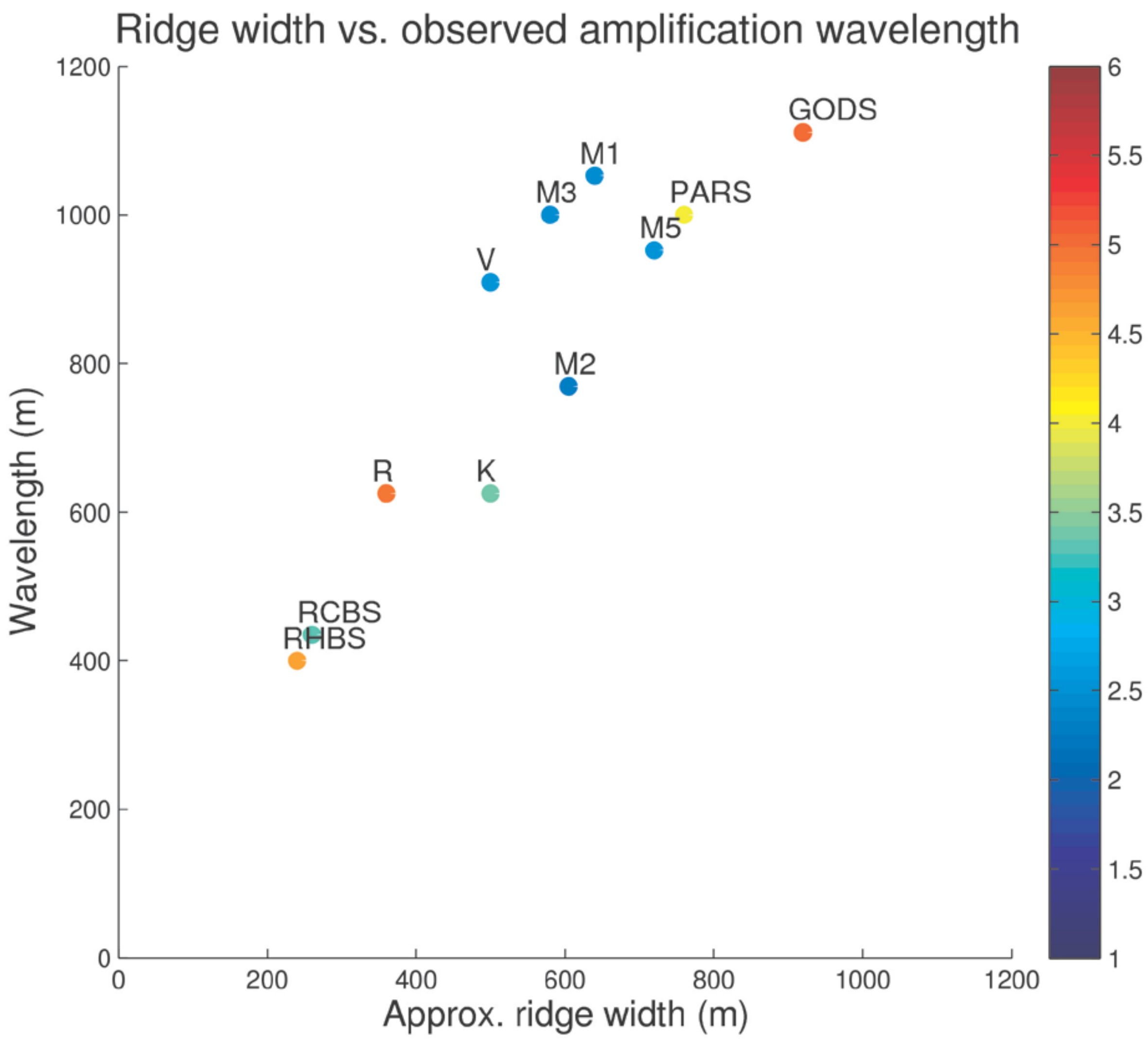

Figure 27 Wavelength of the lowest frequency amplification peak observed in H/V ratios plotted against the approximate width of the ridgeline. Colours indicate the maximum H/V ratio associated with each amplification peak. Wavelength is calculated based on a uniform velocity of 1000 m/s. Ridge width is estimated across the ridge-perpendicular transect closest to the array/station by using the base of the hill deduced from surface topography. Note, that Kinsey ridge exhibits complex topography and ridge width is only approximate. Mt Pleasant stations placed parallel to the ridgeline are plotted separately, whereas arrays traversing perpendicular to ridgelines are plotted as a single point. All stations apart from Vernon Terrace (V) and M1, M2 at Mt Pleasant are located on the ridge crest.

6.0 CONCLUSIONS

Strong and variable ground-motion amplification was observed in the Port Hills, Christchurch, during small to moderate aftershocks of the Canterbury earthquake sequence. Amplification effects were observed over a broad frequency range down to ~1 Hz.

Topographic amplification at 1–3 Hz was consistently observed at ridge-top locations with the estimated wavelength of amplification comparable to and strongly correlated with ridge width. The degree of amplification in this frequency range appears to be linked to ridge shape, with steep, narrow ridges such (e.g., Redcliffs) showing particularly strong amplification. Our results also imply that relatively low-velocity material comprises the eastern Port Hills (also found in down-hole measurements; Massey et al. 2014b), which is thought to have enhanced these amplification effects. The relative and combined contributions of topography and material properties to amplification are being further studied with 2D site-specific modelling (e.g. Massey et al. 2014b).

Amplification at frequencies > 3 Hz varied strongly in degree and polarization over short distances. This amplification was inferred to arise from contrasts in local material properties such as weakened rock/soil layers and/or sharp local convex breaks in slope (e.g., Kinsey Terrace, Redcliffs respectively). Polarization at these sites was observed in the ridge-perpendicular direction (also perpendicular to tensional cracking associated with landslide-prone slopes).

The source back-azimuth was also a factor that likely influenced ground-motion amplification at Redcliffs, although it was less important than the site conditions. Amplification at Redcliffs tended to be greatest when sources were aligned with the major ridge axis, leading to preferential amplification in the ridge-perpendicular direction. No significant dependence on source back-azimuth was found at the other sites.

Average PGA amplification ratios between neighbouring rock sites ranged up to 2.5 for horizontal motions and 3 for vertical motions, but with significant event-to-event variation. Results indicate significant local variability of high-frequency ground motion over short distances in hillside areas. It is important to note, these factors are derived from small to moderate sized earthquakes and may differ in large earthquakes.

Topographic and stratigraphic ground motion amplification effects identified in this study are likely to have contributed to high levels of building damage and permanent ground displacement during the Mw 6.2 February 2011 earthquake observed at ridge-top sites. The results of this study have implications for slope stability assessment and engineering design in hillside areas, given that current New Zealand building codes do not explicitly take into account topographic effects in hillside areas.

7.0 FUTURE DIRECTIONS

This research presented here complements ongoing work investigating slope stability in the Port Hills funded by the Natural Hazards Platform. The frequency-dependent amplification functions provided here, can be incorporated into broadband modelling techniques to estimate the level of ground-shaking at Port Hills sites during large events of the Canterbury sequence. Furthermore, observed site amplification characteristics are being used to further complement and benchmark detailed 2-D numerical models of ground-motion amplification and slope failure during the largest earthquakes to impact the Port Hills (e.g., Massey et al., 2014a; 2014b).

8.0 REFERENCES

Assimaki, D., & Jeong S. (2013). Ground-motion observations at Hotel Montana during the M 7.0 2010 Haiti earthquake: Topography or soil amplification? *Bulletin of the Seismological Society of America, 103*(5): 2577–2590.

Beavan, J., Fielding, E., Motagh, M., Samsonov, S., & Donnelly N. (2011). Fault location and slip distribution of the 22 February 2011 Mw6.2 Christchurch, New Zealand, earthquake from geodetic data. *Seismological Research Letters 82*(6): 789–799.

Bell, D. H., & Trangmar, B. B. (1987). Regolith materials and erosion processes on the Port Hills. *Urban Slope Stability,* New Zealand Geomechanical Society: 93–105.

Bonamasa, O., & J.E Vidale (1991). Directional site resonances observed from aftershocks of the 18 October 1989 Loma Prieta earthquake. *Bulletin of the Seismological Society of America, 81*(5): 1945–1957.

Buech, F., Davies, T. R., Pettinga, J. R. (2010). The Little Red Hill seismic experimental study: Topographic effects on ground motion at a bedrock-dominated mountain ediface. *Bulletin of the Seismological Society of America, 100*(5A): 2219–2229.

Burjánek, J., Gassner-Stamm, G., Poggi, V., & Moore, J. R. (2010). Ambient vibration analysis of an unstable mountain slope. *Geophysical Journal International, 180*: 820–828.

Del Gaudio, V., & Wasowski, J. (2010). Advances and problems in understanding the seismic response of potentially unstable slopes. *Engineering Geology*. doi:10.1016/j.enggeo.2010.09.007.

Forsyth, P. J., Barrell, D. J. A., & Jongens R. (2008). *Geology of the Christchurch area*. Institute of Geological & Nuclear Sciences Limited, 1:250000 geological map 16: 1 sheet + 67 p.

Geli, L., Bard, P.-Y., & Jullien, B. (1988). The effect of topography on earthquake ground motion: A review and new results. *Bulletin of the Seismological Society of America, 78*(1): 42–63.

Gledhill, K. R., Ristau, J., Reyners, M. E.; Fry, B.; Holden, C. (2011). The Darfield (Canterbury, New Zealand) M_w7.1 earthquake of September 2010: A preliminary seismological report. *Seismological Research Letters, 82(3):* 378–386; doi: 10.1785/gssrl.82.3.378

Harp, E. L., & Jibson, R. W. (2002). Anomalous concentrations of seismically triggered rock falls in Pacoima Canyon: Are they caused by highly susceptible slopes or local amplification of seismic shaking? *Bulletin of the Seismological Society of America, 92*(8): 3180–3189.

Hartzell, S., Meremonte, M., Ramírez-Guzmán, L., & McNamara D. (2014). Ground motion in the presence of complex topography: Earthquake and ambient noise sources. *Bulletin of the Seismological Society of America, 104*(1): 451–466.

Heron, D., Lukovic, B., Massey, C., Ries, W., & McSaveney, M. (2014). GIS modelling in support of earthquake-induced rockfall and cliff collapse risk assessment in the Port Hills, Christchurch, *Journal of Spatial Science*, DOI: 10.1080/14498596.2014.913509

Holden, C., Kaiser, A. E., & Massey, C. I. (2014). Observations and analysis of topographic effects in the seismic response of the Port Hills following the 2011 Christchurch earthquake. *Proceedings of the 10NCEE, July 21–25, Anchorage*, Paper 1005 in press.

Hough, S. E., Altidor, J. R., Anglade, D., Given, D., Janvier, M. G., Maharrey, J. Z., Meremonte, M., Mildor, B.S., Prepetit, C., & Yong, A. (2010). Localized damage caused by topographic amplification during the 2010 M 7.0 Haiti earthquake. *Nature Geoscience, 3*(11): 778–782.

Hungr, O., Lerouil, S., & Picarelli, L. (2014). The Varnes classification of landslide types. *Landslides (2014) 11*:167–194. DOI 10.1007/s10346-013-0436-y

Kaiser, A. E., Holden, C., Beavan, R. J., Beetham, R. D., Benites, R. A., Celentano, A., Collet, D., Cousins, W. J., Cubrinovski, M., Dellow, G. D., Denys, P., Fielding, E., Fry, B., Gerstenberger, M. C., Langridge, R. M., Massey, C. I., Motagh, M., Pondard, N., McVerry, G. H., Ristau, J., Stirling, M. W., Thomas, J., Uma, S. R., Zhao, J. X. (2012). The M_w 6.2 Christchurch Earthquake of February 2011: Preliminary report. *New Zealand Journal of Geology and Geophysics, 55(*1): 67–90; doi:10.1080/00288306.2011.641182

Kaiser, A. E., Holden, C., & Massey C. I. (2013a). Determination of site amplification, polarization and topographic effects in the seismic response of the Port Hills following the 2011 Christchurch earthquake. 8 p. IN: Same risks, new realities: New Zealand Society for Earthquake Engineering Technical Conference and AGM, April 26–28, 2013, Wellington. Wellington: New Zealand Society for Earthquake Engineering.

Kaiser, A. E., Oth, A., Benites, R. A. (2013b). Separating source, path and site influences on ground motion during the Canterbury earthquake sequence, using spectral inversions. Paper no. 18 (8 p.) IN: *Same risks, new realities: New Zealand Society for Earthquake Engineering Technical Conference and AGM, April 26–28*, 2013, Wellington. Wellington: New Zealand Society for Earthquake Engineering.

Keefer, D. K. 1984. Landslides caused by earthquakes. *Geological Society of America Bulletin 95*(4): 406–421.

Konno, K., & Ohmachi, T. (1998). Ground-motion characteristics estimated from spectral ratio between horizontal and vertical components of microtremor. *Bull of the Seismological Society of America 88*: 228–241.

Massey, C. I., Yetton, M. J., Carey, J., Lukovic, B., Litchfield, N., Ries, W., & McVerry, G. (2013). Canterbury Earthquakes 2010/11 Port Hills Slope Stability: Stage 1 report on the findings from investigations into areas of significant ground damage (assessed source areas). *GNS Science Consultancy Report 2012/317*. http://www.ccc.govt.nz/homeliving/civildefence/chchearthquake/porthillsgeotech/porthillsmass movement.aspx

Massey, C. I. McSaveney, M. J., Taig, T., Richards, L., Litchfield, N. J., Rhoades, D. A., McVerry, G. H., Lukovic, B., Heron, D. W., Ries, W., & Van Dissen, R. J. (2014a). Determining rockfall risk in Christchurch using rockfalls triggered by the 2010/2011 Canterbury earthquake sequence, New Zealand. *Earthquake Spectra,* special edition on the 2010/11 Canterbury earthquake sequence (doi.org/10.1193/021413EQS026M).

Massey, C. I., Taig, T., Della Pasqua, F., Lukovic, B., Ries, W., & Archibald, G. (2014b). Canterbury Earthquakes 2010/11 Port Hills Slope Stability: Debris avalanche risk assessment for Richmond Hill. *GNS Science Consultancy Report 2014/34*.

Meunier, P., Hovius, N., & Haines, J. A. (2008). Topographic site effects and the location of earthquake induced landslides. *Earth and Planetary Science Letters 275*: 221–232.

Moore, J. R., Gischig, V., Burjanek, J., Loew, S., & Fäh, D. (2011). Site effects in unstable rock slopes: Dynamic behaviour of the Randa Instability (Switzerland). *Bulletin of the Seismological Society of America 101*(6): 3110–3116.

Parolai, S., & Richwalski, S. M. (2004). The importance of converted waves in comparing H/V and RSM site response estimates. *Bulletin of the Seismological Society of America 94*(1): 304–313.

Ristau, J., Holden, C., Kaiser, A. E., Williams, C. A., Bannister, S. C., & Fry, B. (2013). The Pegasus Bay aftershock sequence of the M_w 7.1 Darfield (Canterbury), New Zealand earthquake. *Geophysical Journal International, 195*(1): 444–459; doi: 10.1093/gji/ggt222

Sepúlveda, S. A., Murphy, W., Jibson, R. W., & Petley, D. N. (2005). Seismically induced rock slope failures resulting from topographic amplification of strong ground motions: The case of Pacoima Canyon, California. *Engineering Geology 80*: 336–348.

Standards New Zealand. (2004). *Structural Design Actions – Part 5 Earthquake Actions – New Zealand*. New Zealand Standard NZS 1170.5:2004.

Wartman, J., Dunham, L., Tiwari, B., & Pardel, D. (2013). Landslides in eastern Honshu induced by the 2011 Tohoku Earthquake. *Bulletin of the Seismological Society of America, 103*: 1503–1521, doi: 10.1785/0120120128.

9.0 ACKNOWLEDGEMENTS

This research was funded by the Earthquake Commission as part of the biennial research grant program, with additional funding from the New Zealand Natural Hazards Research Platform. The authors would like to thank GeoNet staff Lara Bland, Caroline Little, Charlie O'Reilly, Todd Chandler and John Young, as well as Tim O'Neil from Christchurch for their excellent efforts managing the seismic arrays. Sandra Bourguignon (GNS Science) provided helpful guidance in the extraction of Taurus data. Nick Horspool (GNS Science) kindly provided the map in Figure 2 illustrating spatial variation of building damage based on data provided by the Earthquake Commission. We also thank Dave Heron (GNS Science) for generating the GIS-based maps of the sites in Figure 4–Figure 7. Mauri McSaveney and Rafael Benites (GNS Science) provided helpful constructive reviews of this report.

www.gns.cri.nz

Principal Location

1 Fairway Drive
Avalon
PO Box 30368
Lower Hutt
New Zealand
T +64-4-570 1444
F +64-4-570 4600

Other Locations

Dunedin Research Centre
764 Cumberland Street
Private Bag 1930
Dunedin
New Zealand
T +64-3-477 4050
F +64-3-477 5232

Wairakei Research Centre
114 Karetoto Road
Wairakei
Private Bag 2000, Taupo
New Zealand
T +64-7-374 8211
F +64-7-374 8199

National Isotope Centre
30 Gracefield Road
PO Box 31312
Lower Hutt
New Zealand
T +64-4-570 1444
F +64-4-570 4657